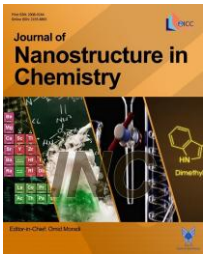

J. Nanostruct Chem. 2026; 16(2): 188-211

Journal of Nanostructure in Chemistry (JNSC)

https://doi.org/10.57647/jnsc.2026.1602.10

Research Article

# A Comparative Study of Synergistic Effects of Biogenic Nanoparticles and Plant Extracts in Tragacanth and Carboxymethyl Tragacanth-based Edible Films for Preserving Raw Pistachios

Zohre Jafari Vafa [1], Ehsan Nazarzadeh Zare [2,*], Ali Najafi[3], Taotao Zhao[4,*]

[1] *School of Physics, Damghan University, Damghan 36716-45667, Iran*
[2] *School of Chemistry, Damghan University, Damghan 36716-45667, Iran*
[3] *Department of Food Science and Technology, Da.C., Islamic Azad University, Damghan, Iran*
[4] *The Quzhou Affiliated Hospital of Wenzhou Medical University, Quzhou People's Hospital, 3240009, Quzhou, Zhejiang, China*

* **Corresponding authors:** 344607699@wmu.edu.cn, ehsan.nazarzadehzare@gmail.com, e.nazarzadeh@du.ac.ir

**Article History:**

Received:
19 October 2025

Revised:
16 December 2025

Accepted:
28 February 2026

Published in Issue:
30 April 2026



**Abstract**

Bio-based nanocomposite films were developed using poly(vinyl alcohol) (PVA) reinforced with tragacanth gum (TG) and carboxymethyl tragacanth (CMT), incorporating biogenic ZnO or CuO nanoparticles and plant-derived extracts (cinnamon or clove). A comparative evaluation of structural, surface, mechanical, and oxygen barrier properties was conducted to assess their potential for active food packaging. FESEM analysis revealed that CMT-based films possessed a more homogeneous and compact microstructure with fewer microcracks compared to TG-based films. The lower contact angle observed for CMT-containing films indicated stronger intermolecular interactions and a denser polymer network. CMT-based films demonstrate a more favorable balance between strength and elongation, resulting in improved toughness and mechanical stability, which are critical for flexible food packaging applications. Oxygen permeability measurements demonstrated that optimized CMT-based film achieved a lower oxygen transmission rate (26.80 $cm^3/m^2 \cdot 24\ h \cdot 0.1$ MPa) than TG-based film (27.53 $cm^3/m^2 \cdot 24\ h \cdot 0.1$ MPa), despite reduced thickness (70 µm versus 78 µm). Analysis of diffusion and solubility coefficients indicated that reduced oxygen solubility within the CMT matrix ($2.66 \times 10^{-10}$ $cm^3/cm^2.cm.Pa$) was the dominant factor governing overall permeability. The practical performance of the films was further assessed by coating raw pistachios. The optimized CMT-based film preserved the visual quality of pistachios for up to 12 days under ambient conditions without observable deterioration. These results highlight CMT-based nanocomposite films as promising sustainable materials for oxygen-sensitive food packaging applications.

**Keywords:** Active food packaging; Biogenic ZnO and CuO nanoparticles; Carboxymethyl tragacanth; Plant-derived antioxidants; Pistachio preservation; Tragacanth gum

**Cite this article:** Jafari Vafa Z., Nazarzadeh Zare E., Najafi A., Zhao T. A Comparative Study of Synergistic Effects of Biogenic Nanoparticles and Plant Extracts in Tragacanth and Carboxymethyl Tragacanth-based Edible Films for Preserving Raw Pistachios. *J Nanostruct Chem* **16**, 188-211 (2026). https://doi.org/10.57647/jnsc.2026.1602.10

## Graphical abstract

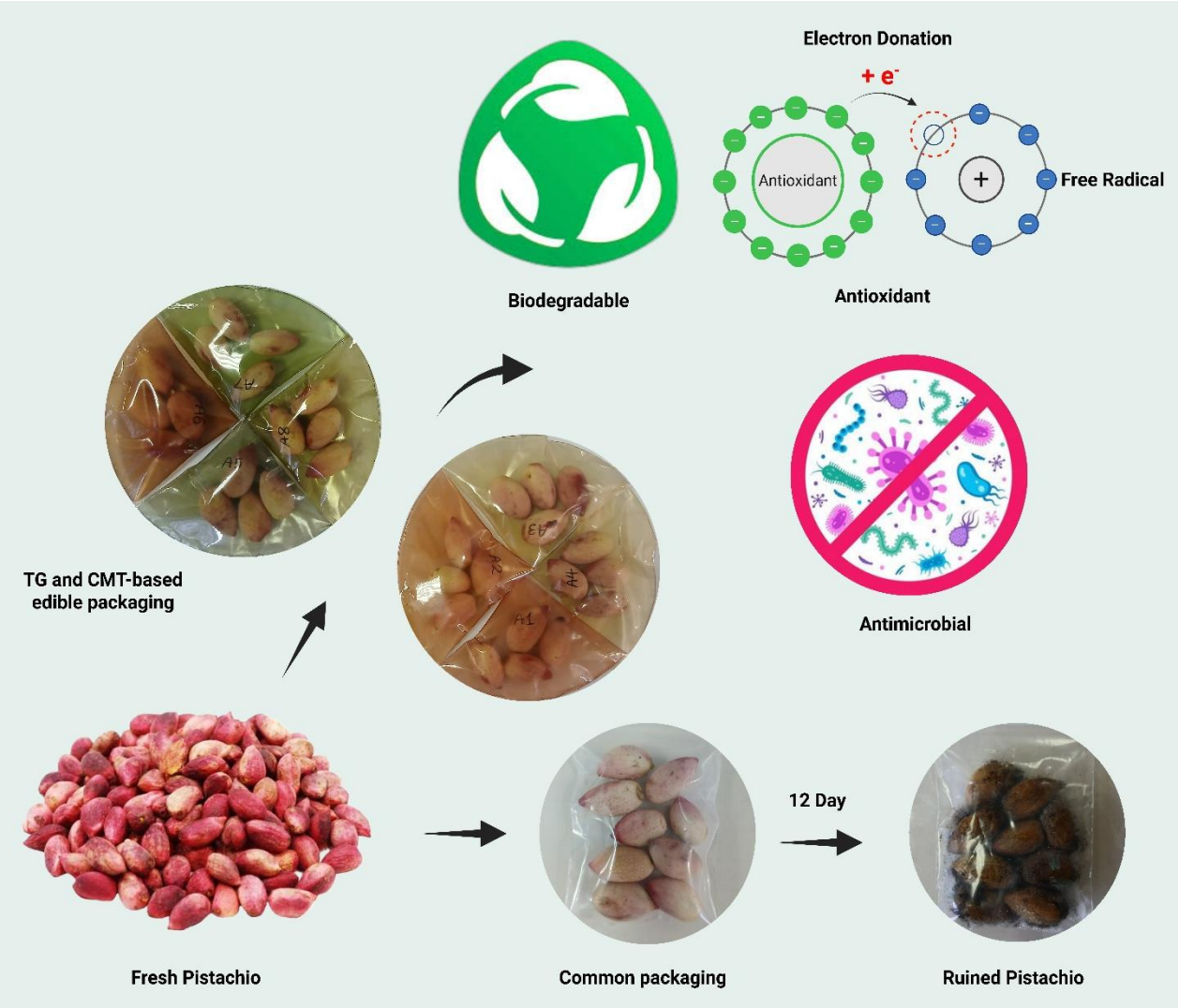


## 1. Introduction

The increasing global demand for sustainable, biodegradable, and safe food packaging materials has accelerated research on edible films derived from natural polymers [1]. Tragacanth gum (TG), a natural exudate polysaccharide, and its derivative carboxymethyl tragacanth (CMT) have attracted considerable attention due to their excellent film-forming ability, high biocompatibility, and biodegradability [2]. These biopolymers can form cohesive, flexible films suitable for packaging applications, particularly for perishable food products such as nuts and fruits. However, native TG and CMT films often exhibit limitations in mechanical strength, and antimicrobial performance, which restrict their practical application.

Raw pistachios are among the most economically valuable tree nuts worldwide, owing to their high consumer demand, export significance, and rich nutritional profile, including unsaturated fatty acids, proteins, minerals, and bioactive compounds. Despite these advantages, raw pistachios are highly susceptible to quality deterioration during storage due to their high lipid content, which promotes oxidative rancidity, as well as their vulnerability to microbial contamination under inappropriate storage conditions. Lipid oxidation not only leads to off-flavors and reduced sensory quality but also decreases nutritional value, while microbial growth poses serious food safety concerns. Lipid oxidation and deteriorative reactions in pistachio nuts are accelerated during storage, especially at higher temperatures and longer times, affecting fat quality factors [3]. Consequently, extending the shelf life of raw pistachios requires packaging systems that simultaneously provide effective oxygen and moisture barriers, antioxidant protection, and antimicrobial functionality [4]. These challenges highlight the urgent need for advanced, sustainable, and multifunctional packaging materials tailored specifically for pistachio preservation [5].

Recent studies have explored the incorporation of functional additives into polysaccharide-based films to overcome these limitations. Metal oxide nanoparticles,

10.57647/jnsc.2026.1602.10

particularly zinc oxide (ZnO) and copper oxide (CuO), have been widely reported for their broad-spectrum antimicrobial activity, UV-blocking properties, and potential to reinforce the polymer matrix [6-9].

In parallel, plant-derived bioactive compounds, including clove and cinnamon extracts, are recognized for their antioxidant and antimicrobial properties. Several researchers have demonstrated that integrating plant extracts into edible films can significantly enhance their functionality, including reducing lipid oxidation, inhibiting microbial growth, and improving shelf life of packaged foods [10-13]. Despite these advances, most studies have focused on either nanoparticles [14] or plant extracts [11-13] individually, with limited investigations into their combined or synergistic effects in biopolymer matrices. Few studies have compared the performance of TG- and CMT-based films incorporating both biogenic nanoparticles and plant extracts, and systematic evaluations of their physicochemical, mechanical, and antimicrobial properties in the context of real food preservation remain scarce. Such comparative studies are crucial to understand how different polymer matrices and bioactive fillers interact, enabling the design of optimized films for specific food applications.

Therefore, this study for the first time systematically compares edible films based on TG and CMT, incorporating biogenic ZnO and CuO nanoparticles in combination with clove and cinnamon extracts. The research evaluates the physicochemical, structural, mechanical, antimicrobial, and antioxidant properties of the films, with a particular emphasis on their barrier performance and functional efficacy for preserving raw pistachios. By investigating the synergistic effects of nanoparticles and plant extracts, this study provides insights into the development of advanced, functional, and sustainable edible films for food packaging applications.

## 2. Experimental

### 2.1. Materials

Tragacanth gum with a ribbon-like morphology was obtained from Sigma Aldrich. The gum is composed of approximately 60–70% basurin and 30–40% tragacanthine. A 2% aqueous solution of tragacanth gum exhibits a viscosity between 2.8 and 28 centipoise, and the polymer has a molecular weight of approximately 8.40 × $10^5$ Daltons. Polyvinyl alcohol (PVA, 98-99%, $M_w$=145000 g/mol), Citric acid monohydrate (CA, ≥99.0%), and glycerol (Gly, ≥99.5%, $M_w$=92.10 g/mol), zinc acetate dihydrate (99.5%), copper(II) sulfate pentahydrate ($CuSO_4.5H_2O$, 99.0-100%), Sodium hydroxide (NaOH, ≥98%) and monochloroacetic acid (Chloroacetic acid, ≥99.0%) were purchased from Merck Company (Germany). Plant materials including clove (*Syzygium aromaticum*), cinnamon (*Cinnamomum cassia*), and green pistachio peel (*Pistacia vera*) were used to prepare the natural extracts. Ethanol (≥95.0%, Merck, Germany) was used as the extraction solvent in the Soxhlet apparatus. The dried extracts were stored at 4 °C and later incorporated into the polymeric film formulations. 2,2-Diphenyl-1-picrylhydrazyl (DPPH, $M_w$=394.32 g/mol) for antioxidant test was purchased from Sigma-Aldrich company.

### 2.2. Characterization

### 2.3. Preparation of plant extracts

Natural extracts were obtained from clove (*Syzygium aromaticum*), cinnamon (*Cinnamomum cassia*), and fresh green pistachio hull (*Pistacia vera*). The dried and powdered plant materials (25 g) were extracted with ethanol using a Soxhlet apparatus for 6 hours (Fig. 1A). Ethanol was used in a sufficient amount to fully immerse the plant material and ensure continuous reflux and proper Soxhlet cycling. The obtained extracts were filtered and concentrated under reduced pressure to remove the solvent and then stored at 4 °C in dark bottles for further use [15]. Clove and cinnamon extracts were selected due to their high content of well-known bioactive compounds, primarily eugenol in clove and cinnamaldehyde in cinnamon. These compounds exhibit strong antimicrobial and antioxidant activities and have been extensively reported as effective natural preservatives in food packaging systems. Moreover, both extracts are generally recognized as safe (GRAS) and demonstrate good compatibility with polymeric matrices, making them suitable candidates for active food packaging applications [16-21].

### 2.4. Green synthesis of nanoparticles

Zinc oxide (ZnO) nanoparticles were synthesized via a green synthesis approach using green pistachio peel extract as a reducing and stabilizing agent, following the method described by [22], whereas copper oxide (CuO) nanoparticles were prepared using the same extract through a green synthesis procedure reported by [23] (Fig. 1B).

*ZnO Nanoparticles*: Initially, 0.2 g of green pistachio peel extract was dissolved in 70 mL of distilled water. Subsequently, 60 mL of the aqueous solution was added dropwise to a 0.1 M Zinc acetate solution under continuous stirring. After 1 h of stirring, the color of the solution changed to cream-colored, indicating the occurrence of the reaction. The stirring was continued for 3 h, after which the pH of the solution was adjusted to 12

by the addition of 0.1 M sodium hydroxide (NaOH) solution. Upon gradual addition of NaOH, the color of the solution changed from cream-color to dark yellow, and the formation of a yellow precipitate was observed, indicating the presence of zinc oxide nanoparticles. After stirring for an additional 30 min, the suspension containing the precipitate was centrifuged several times at 4000 rpm for 15 min.

The collected precipitates were repeatedly washed with deionized water until a neutral pH was achieved. The resulting precipitate was then dried at 80 °C for 5 h, yielding a light brown powder. A portion of the dried powder was dispersed in a few milliliters of distilled water and subjected to ultrasonication for 1 h to ensure complete dispersion of the particles. The suspension was subsequently transferred into an autoclave and heated in an oven at 180 °C for 36 h. After cooling to room temperature, the autoclave was opened, the solution was filtered, and the obtained precipitate was dried at ambient temperature.

*CuO Nanoparticles:* Similar to the previous synthesis, 0.2 g of green pistachio peel extract was first dissolved in 70 mL of distilled water. Subsequently, 60 mL of a 0.1 M copper(II) sulfate ($CuSO_4.5H_2O$) solution, which exhibited a light blue color, was prepared. The pistachio peel extract solution was then added dropwise to the $CuSO_4.5H_2O$ solution under continuous stirring. During the addition, the color of the solution gradually changed to sea green and finally to light green. The mixture was stirred for 1 h and then gently heated to 80 °C to ensure completion of the reaction and initiate nanoparticle precipitation.

The solution was subsequently kept at room temperature for 2–3 h to allow the nanoparticles to settle. With increasing temperature, the color of the solution changed from light green to dark green resulting in the formation of a brownish precipitate after sedimentation. The obtained precipitate was collected by filtration and washed several times with deionized water and ethanol to remove residual impurities.

Finally, the collected precipitates were dried at 80 °C for 5 h, yielding a black-colored powder. ZnO and CuO nanoparticles were selected due to their well-documented antimicrobial efficacy, complementary mechanisms of action, and suitability for food-related applications. ZnO nanoparticles primarily exert antimicrobial activity through the generation of reactive oxygen species (ROS) and disruption of bacterial cell membranes [24, 25], while CuO nanoparticles additionally release $Cu^{2+}$ ions that interfere with intracellular enzymes and metabolic pathways.

The combination of these mechanisms enhances broad-spectrum antimicrobial performance. Moreover, ZnO is generally recognized as safe (GRAS) by regulatory authorities, and CuO has demonstrated low toxicity at controlled concentrations, making both nanoparticles promising candidates for active food packaging systems [26]. In addition to their antimicrobial function, ZnO and CuO nanoparticles act as effective reinforcing agents, improving the mechanical strength and barrier properties of polymeric matrices through strong interfacial interactions and improved stress transfer [25].

### 2.5. Carboxymethylation of tragacanth gum

Carboxymethylation of tragacanth gum (TG) to obtain sodium Carboxymethyl Tragacanth (CMT) was carried out following the procedure described by [13] (Fig. 1C). Initially, 1 g of TG was added to 100 mL of deionized water and stirred vigorously until a clear and homogeneous solution was obtained. Subsequently, 1.2 g of NaOH was dissolved in 10 mL of deionized water and added to the TG solution. The temperature of the mixture was raised to 50 °C and maintained under continuous stirring for 30 min. In the next step, 1.3 g of chloroacetic acid was dissolved in 10 mL of deionized water and added to the TG+NaOH solution. The resulting mixture was stirred at 50 °C for 4 h. After cooling, ethanol was added in an amount twice the volume of the final solution to induce the precipitation of CMT. The precipitate was collected and dried at 40 °C for 24 h.

### 2.6. Film preparation

In this study, nanocomposite films based on TG and CMT (under the optimized equal-proportion (50:50) formulation) were fabricated. The 50:50 (w/w) ratio of TG:PVA and CMT:PVA was selected to achieve a balanced combination of the excellent film-forming ability and mechanical integrity of PVA with the functional properties of TG and CMT, such as biodegradability and enhanced interactions with nanoparticles and plant extracts. Although neat PVA films exhibit high structural integrity, incorporating TG or CMT at an equal proportion enables the formation of networks with improved functional performance while maintaining sufficient mechanical strength and film homogeneity. Primary formulation observations confirmed that this ratio provided uniform films with reproducible properties suitable for packaging applications. Various nanoparticles (ZnO and CuO) and plant extracts (clove and cinnamon) were simultaneously used as fillers. Initially, 0.5 g of TG (or CMT) was added to 50 mL of deionized water and stirred at high speed for 20 minutes to obtain a viscous solution. In a separate container, 0.5 g of polyvinyl alcohol (PVA) was dissolved in 40 mL of deionized water under a closed lid at 90 °C for 30 minutes to obtain a clear solution.

10.57647/jnsc.2026.1602.10

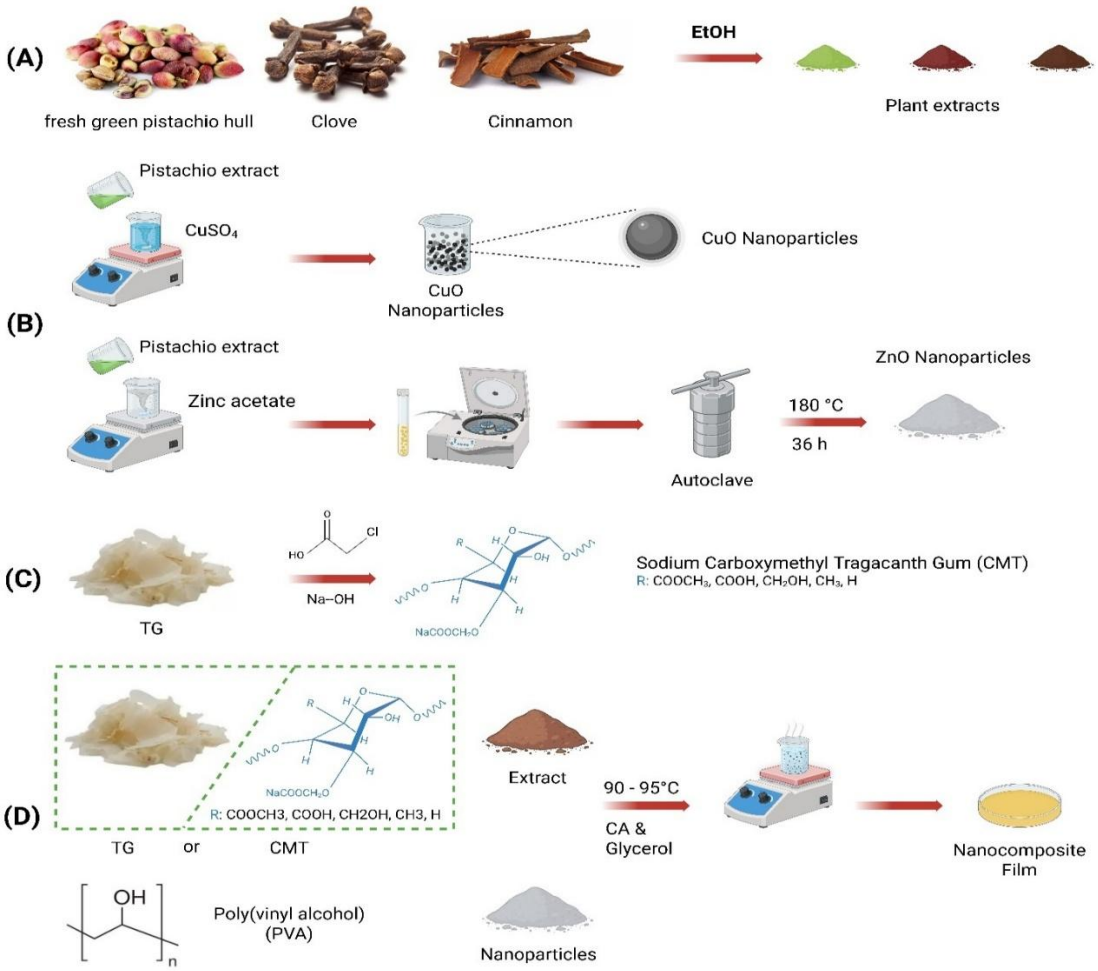


**Figure 1.** Synthesis steps of nanocomposite films, (A) Extraction of pistachio green hull, clove, and cinnamon extracts, (B) Green synthesis of CuO and ZnO nanoparticles using pistachio green hull extract, (C) Carboxymethylation of tragacanth gum, and (D) Preparation of nanocomposite films based on TG and CMT

**Table 1.** The different amounts of extracts and nanoparticles used, and the codes assigned to each sample

| Sample code | Base gum | % | Base Polymer | % | Nanoparticle | Nanoparticle percentage (%)* | Extract | Extract percentage (%)* |
|---|---|---|---|---|---|---|---|---|
| T | TG | 50 | PVA | 50 | -- | -- | -- | -- |
| T1 | TG | 50 | PVA | 50 | ZnO | 5 | Cinnamon | 7 |
| T2 | TG | 50 | PVA | 50 | ZnO | 3 | Cinnamon | 7 |
| T3 | TG | 50 | PVA | 50 | ZnO | 5 | Clove | 7 |
| T4 | TG | 50 | PVA | 50 | ZnO | 3 | Clove | 7 |
| T5 | TG | 50 | PVA | 50 | CuO | 5 | Cinnamon | 7 |
| T6 | TG | 50 | PVA | 50 | CuO | 3 | Cinnamon | 7 |
| T7 | TG | 50 | PVA | 50 | CuO | 5 | Clove | 7 |
| T8 | TG | 50 | PVA | 50 | CuO | 3 | Clove | 7 |
| C | CMT | 50 | PVA | 50 | -- | -- | -- | -- |
| C1 | CMT | 50 | PVA | 50 | ZnO | 5 | Cinnamon | 7 |
| C2 | CMT | 50 | PVA | 50 | ZnO | 3 | Cinnamon | 7 |
| C3 | CMT | 50 | PVA | 50 | ZnO | 5 | Clove | 7 |
| C4 | CMT | 50 | PVA | 50 | ZnO | 3 | Clove | 7 |
| C5 | CMT | 50 | PVA | 50 | CuO | 5 | Cinnamon | 7 |
| C6 | CMT | 50 | PVA | 50 | CuO | 3 | Cinnamon | 7 |
| C7 | CMT | 50 | PVA | 50 | CuO | 5 | Clove | 7 |
| C8 | CMT | 50 | PVA | 50 | CuO | 3 | Clove | 7 |

* Relative to the total weight of polymer and base gum (TG/CMT+PVA)

10.57647/jnsc.2026.1602.10

The PVA solution was then added to the TG (or CMT) solution and stirred for an additional 15 minutes. According to Table 1, 7 wt% (Relative to the total weight of TG/CMT+PVA) of the plant extracts and 3 or 5 wt% (Relative to the total weight of TG/CMT+PVA) of the nanoparticles were dispersed in 20 mL of deionized water. First, the extract solution was added to the TG (or CMT) + PVA solution, and the mixture was stirred on a magnetic stirrer for 15 minutes. Then, the nanoparticle suspension was added and stirring continued. Subsequently, 15 wt% (Relative to the total weight of TG/CMT+PVA) citric acid was introduced as a cross-linking agent, followed by 25 wt% (Relative to the total weight of TG/CMT+PVA) glycerol as a plasticizer. The different amounts of extracts and nanoparticles used, as well as the codes assigned to each sample, are listed in Table 1. The final mixture was transferred to an oil bath and heated at 90–95 °C for 2 hours under continuous stirring to obtain the final gel. The resulting gel was then cast into Petri dishes and dried at 40 °C for 24 hours. After drying, the final films were peeled off from the dishes and stored for further analysis (Fig. 1D).

## 3. Results and discussion

Considering the large number of samples and the extensive set of characterization images obtained, only the images corresponding to T1, T3, T5, and T7 (TG series) and C1, C3, C5, and C7 (CMT series), which were expected to exhibit superior properties, are presented in the main manuscript. The complete set of images and characterization results for the remaining samples, including T, T2, T4, T6, T8 and C, C2, C4, C6, C8, has been provided in the Supporting Information. However, in all sections where the results are presented in the form of graphs, quantitative analyses, or statistical evaluations, the data for all samples have been included in the main manuscript to ensure comprehensive comparison and accurate interpretation. This approach was adopted to avoid excessive visual content in the main text while maintaining full analytical transparency.

### 3.1. FTIR-ATR analysis

FTIR-ATR analysis was performed to investigate the chemical structure and evaluate the interactions between different components of the nanocomposite films including PVA, TG, CMT, citric acid, glycerol, ZnO and CuO, and cinnamon and clove plant extracts. The FTIR-ATR spectra of the TG (T series) and CMT (C series) based films are presented in Fig. 2A and Fig. 2B and the FTIR-ATR spectra of the base films are presented in Fig. S1. As can be seen in Fig. S1, both the TG and CMT based films have a broad absorption band in the range of 3200–3500 $cm^{-1}$, which is attributed to the stretching vibrations of the hydroxyl groups (O–H). This band is due to the presence of –OH groups in PVA, TG or CMT, glycerol and citric acid and its width indicates the formation of strong hydrogen bonds between polymer chains [27]. The peak appearing in the range of 2920–2940 $cm^{-1}$ is related to the C–H stretching vibrations of the aliphatic $–CH_2$ groups in the polymer backbone [27]. Also, the absorption band located in the range of 1710–1735 $cm^{-1}$ is assigned to the stretching vibration of the carbonyl (C=O) groups of the ester, which confirms the occurrence of a cross-linking reaction between citric acid and the hydroxyl groups of PVA and gums and the formation of ester bonds [28]. In TG-based films, the band observed in the region of 1600–1650 $cm^{-1}$ is attributed to bound water and the asymmetric stretching vibration of the carboxylate groups of polysaccharides. The intensity of this band increases in CMT-based films, which is due to the presence of carboxymethyl ($–COO^-$) groups, confirming the successful chemical modification of tragacanth. In addition, the peaks in the range of 1020–1150 $cm^{-1}$ are related to the stretching vibrations of C–O–C and C–O bonds and are characteristic of the polysaccharide structure of the gums and PVA chains [29]. The addition of ZnO and CuO nanoparticles to the films (samples T1–T8 and C1–C8) leads to changes in the intensity of the bands and slight shifts in the position of the peaks, indicating the interaction between the nanoparticles and the polymer matrix (Fig. 2A, Fig. 2B and Fig. S1). The presence of ZnO is confirmed by the appearance of bands in the region of 400–550 $cm^{-1}$, which are related to Zn–O stretching vibrations [30], while CuO-containing films show distinct bands in the range of 500–600 $cm^{-1}$, which are attributed to Cu–O vibrations [31]. Also, the broadening and shifting of the O–H band indicates the formation of hydrogen bonds and coordination interactions between the metal oxide nanoparticles and the hydroxyl or carboxyl groups present in the polymer matrix. The addition of cinnamon and clove plant extracts (7 wt%) also causes changes in the FTIR-ATR spectra. New or intensified bands in the range of 1510–1600 $cm^{-1}$ are attributed to the stretching vibrations of aromatic C=C bonds of phenolic compounds such as cinnamaldehyde and eugenol. Also, the bands appearing in the region of 1260–1310 $cm^{-1}$ are related to the C–O stretching vibrations of phenolic groups and confirm the successful presence of plant extracts in the structure of the films. These compounds mainly interact with the polymer chains through hydrogen bonds and help improve the structural stability and functional properties of the films. Overall, the higher absorption intensity of CMT-based films in the carboxylate region (1600–1650 $cm^{-1}$) compared to TG-based films indicates that carboxymethylation has increased the number of $–COO^-$ groups and enhanced the

10.57647/jnsc.2026.1602.10

intermolecular interactions with nanoparticles and plant extracts. These results confirm the successful formation of nanocomposite films with strong interactions between components.

### 3.2. XRD analysis

To investigate the structural and crystalline characteristics of polymeric films based on TG and CMT intended for food packaging, X-ray diffraction (XRD) analysis was performed using a Bruker device (Advanced-Bruker D8, Germany). This analysis allows for the identification of crystalline and amorphous phases, evaluation of the effects of nanoparticles and plant extracts on the polymer network structure, and assessment of changes in the internal order of the films. Fig. 2C and Fig. S2(A) (In the Supplementary Information) show the XRD patterns of the neat (T) and nanocomposite (T1–T8) films based on TG. In these Figures, all samples exhibit a broad peak around ~20°, which indicates the amorphous structure of the films, consistent with the polysaccharide nature of TG matrix. This broad peak is typically attributed to the interlayer spacing of polymer chains or the short-range order within the polymer matrix [32]. It should be noted that the characteristic diffraction peaks of ZnO and CuO are not clearly distinguishable in the XRD patterns of the composite films, which can be attributed to their low loading levels (3 and 5 wt%), small particle size, and uniform dispersion within the predominantly amorphous polymer matrix, leading to peak broadening and overlap with the polymer halo. The shape and width of this peak, rather than absolute intensity, are used to qualitatively assess changes in structural order. Variations in peak width and shape among the samples suggest that incorporation of nanoparticles and plant extracts leads to a disruption of polymer chain packing, increasing short-range disorder within the TG network.

Fig. 2D and Fig. S2(B) (In the Supplementary Information) show the XRD patterns of the neat (C) and nanocomposite (C1–C8) films based on CMT. The XRD pattern of the CMT material (Fig. S3 in the Supplementary Information) indicates its semi-crystalline structure [13]. As shown in Fig. S2(B) (In the Supplementary Information), the neat CMT-based film (sample C) exhibits a semi-crystalline structure; however, the nanocomposite films display a broad and dominant peak in the range of 2θ≈20°–22°, confirming the amorphous nature of the polymer matrix. The broadening and shape variations of this peak in some samples containing nanoparticles and extracts, compared to sample C, indicate a disturbance in the short-range arrangement of polymer chains, likely due to physical interference and the dispersion of additives within the polymer matrix [13].

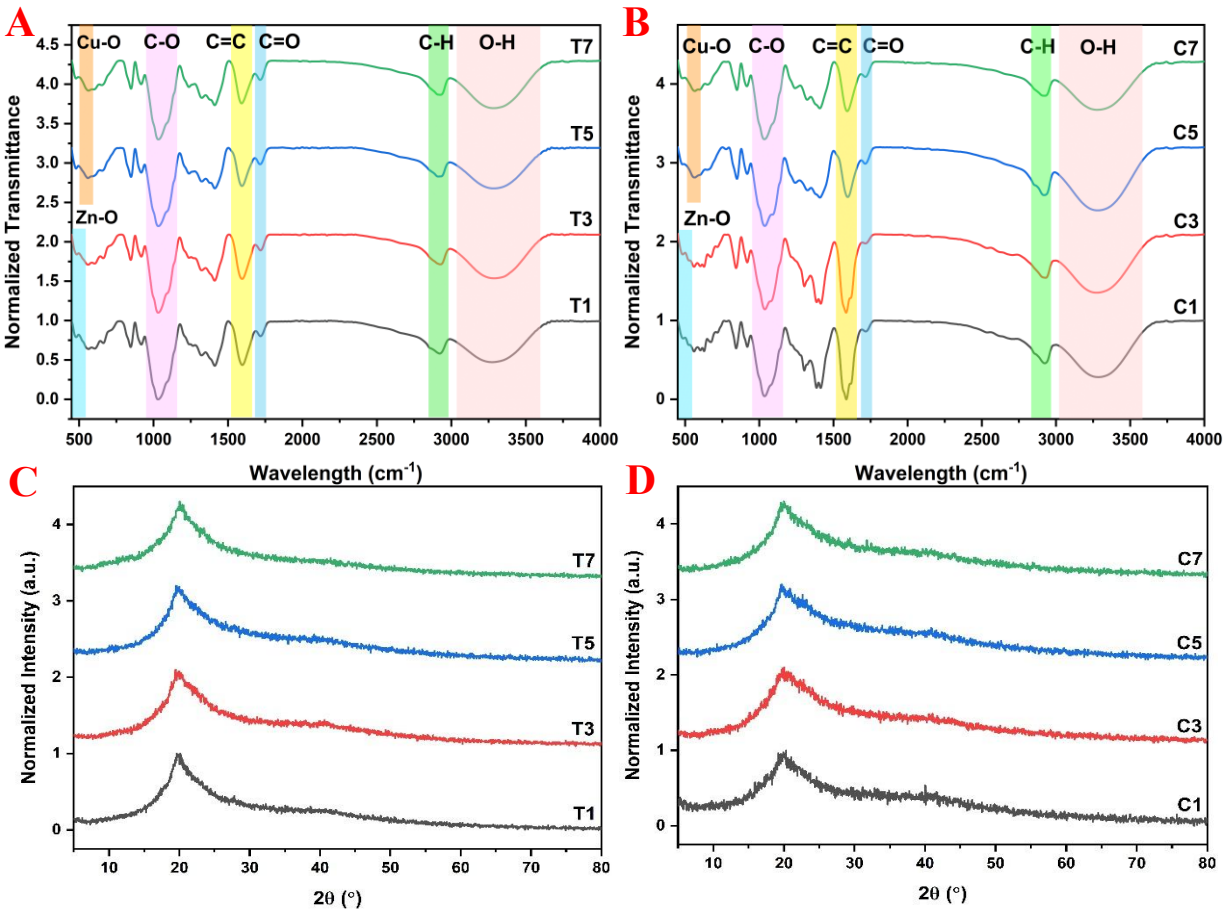


**Figure 2.** FTIR-ATR spectra and XRD patterns of nanocomposite films based on (A, C) TG (T series) and (B, D) CMT (C series)

10.57647/jnsc.2026.1602.10

Comparison among the samples shows that sample C2 exhibits a relatively sharper peak with higher intensity, indicating partial preservation of short-range order within the CMT structure, possibly due to a more uniform distribution of additives. In contrast, samples C1 and C8 display broader peaks, reflecting a higher degree of amorphousness. These structural variations can directly influence the functional properties of the films—including their mechanical characteristics and thermal behavior. Therefore, the XRD results confirm that the nanoparticle and extract additives significantly modify the structural order of CMT, thereby affecting the macroscopic properties of the resulting films. For the XRD patterns of the constituent components of the nanocomposite films, see Fig. S3 in the Supplementary Information.

Overall, the XRD comparison between the two matrices indicates that CMT exhibits a more stable and robust structure than TG and shows lower amorphization in response to disturbances caused by the additives. In contrast, TG undergoes a rapid decrease in crystallinity and peak broadening. These differences may be attributed to variations in the degree of branching, the presence of carboxymethyl groups, and differences in intermolecular interactions that influence chain packing and structural stability. These factors ultimately affect the mechanical properties and barrier performance of the nanocomposite films based on these matrices (see Sections 3.4 and 3.11). Importantly, our analysis focuses on peak shape and width rather than absolute intensity, avoiding direct comparison of peak intensities between samples for crystallinity evaluation. This approach allows a reliable qualitative assessment of structural disorder and polymer chain arrangement, supported by complementary SEM and FTIR-ATR analyses.

### 3.3. Surface morphology study

The surface morphology was examined using field-emission scanning electron microscopy (FESEM; Sigma 300 VP, ZEISS, Germany). Fig. 3 and Fig. S5 present FESEM images of the TG-based (T series) and CMT-based (C series) films at different magnifications, respectively. Also, Fig. S4 presents FESEM images of the individual components used in the nanocomposite films.
The images of the TG-based films (T series) show that the neat film (T) exhibits a relatively smooth and uniform surface at the microscale, whereas the incorporation of ZnO/CuO nanoparticles and plant extracts induces pronounced morphological changes. These modifications appear as small particle agglomerates and localized surface heterogeneities, which manifest in the form of a more granular texture, increased surface roughness, and larger clusters. Such microstructural inhomogeneities can create stress concentration points and reduce the local mechanical integrity of the film, and by generating preferential diffusion pathways and disrupting the local ordering of polymer chains, they can also affect the barrier properties and thermal stability of the material [33, 34]. Analysis of the C–C8 images demonstrates that the CMT-based films exhibit a more uniform and mechanically robust surface compared to the TG-based films. The well-defined cellular pattern observed in the CMT films containing ZnO fillers (C1–C4) indicates a more controlled shrinkage and improved network formation. Although nanoparticle agglomeration is present in the CMT-based samples, it generally appears on a larger scale with clearly defined boundaries (e.g., in C5 and C6). In contrast, in the TG-based films, the matrix–nanoparticle interactions more frequently lead to granular surface textures and dispersed microcracks (as seen in T1, T3, T5, and T7). The CMT films also show a higher capability to maintain surface integrity, and even after incorporating additives, they display fewer cracks than the TG-based films (except for sample C8). Moreover, the CMT-based samples typically exhibit larger and more well-defined crystalline domains, which may be attributed to stronger interactions between the carboxymethyl groups and the incorporated nanoparticles [35, 36].

Overall, a comparative examination of the CMT-based films (samples C-C8) indicates that the surface morphology of CMT exhibits a denser, more uniform, and structurally more stable network compared to TG-based films. FESEM images show that the CMT matrix, after the incorporation of ZnO/CuO nanoparticles and plant extracts, undergoes only limited disruptions and still maintains its continuous polymeric structure with fewer cracks and lower surface roughness. Even in samples with higher nanoparticle concentrations (such as C1, C3, C5, C7), the CMT network retains its integrity, and the fillers are more uniformly distributed within the matrix. This behavior suggests that CMT is inherently more resistant to morphological degradation, whereas TG films, under the same additives, rapidly lose their structural order and experience significant spreading or structural failure. The higher stability of CMT can be attributed to its greater degree of branching, the presence of carboxymethyl groups, and its higher capacity for hydrogen bonding—factors that ultimately enhance the mechanical properties, and barrier performance of the resulting nanocomposite films [37, 38]. Elemental mapping and quantitative elemental analysis were carried out by EDS integrated into the FESEM (Sigma 300 VP, ZEISS, Germany). Fig. S6 and Fig. S7 (in the supplementary information) show the EDS spectra of the neat and nanocomposite films based on TG and CMT, respectively. The neat films (T and C) consist of two elements, carbon (C) and oxygen (O), whereas the nanocomposite films contain C, O, zinc (Zn), copper (Cu), sodium (Na), potassium (K), and

calcium (Ca). The presence of Na, K, and Ca is attributed to the plant extracts incorporated into the nanocomposite films. Fig. S8 and Fig. S9 (in the supplementary information) present the elemental mapping images of the neat and nanocomposite films based on TG and CMT, respectively. The elemental mapping analyses (Fig. S8 and Fig. S9) reveal clear differences in the distribution of nanoparticles within the TG- and CMT-based films. In the TG series, the neat film (T) shows uniform distributions of C and O, whereas the nanocomposite samples exhibit the expected elemental signatures of Zn or Cu together with Na, K, and Ca originating from the plant extracts.

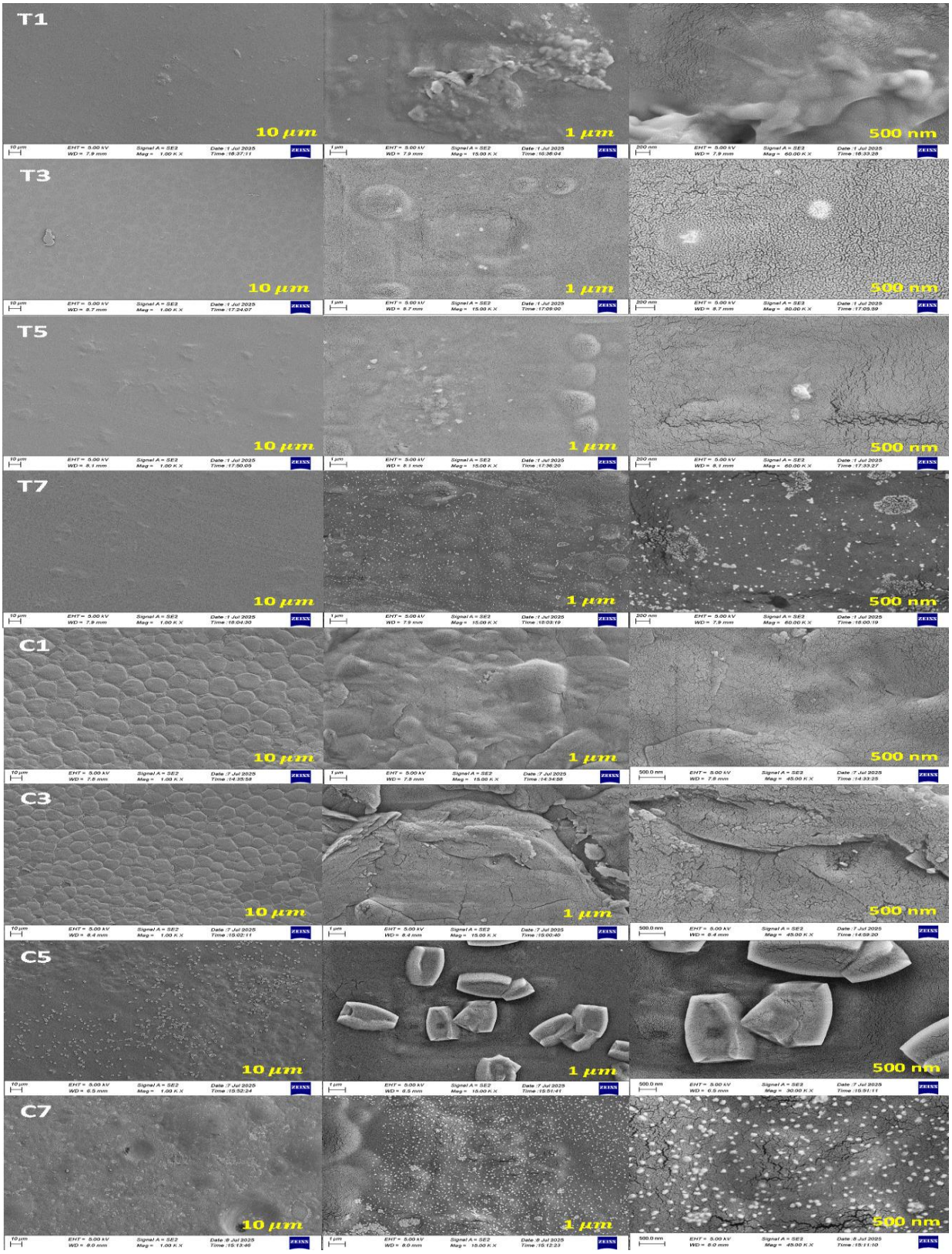


**Figure 3.** SEM micrograph of nanocomposite films based on TG (T series) and CMT (C series)

10.57647/jnsc.2026.1602.10

Although ZnO-containing films (T1, T3) display relatively homogeneous Zn dispersion with only small localized clusters, the CuO-containing films (T5, T7) show more pronounced agglomeration, particularly in T5, where large Cu-rich domains appear. In contrast, the CMT-based films demonstrate significantly more uniform elemental distributions. The Zn- and Cu-containing samples (C1–C7) show well-dispersed nanoparticles with much smaller and fewer aggregation sites, and the matrix remains continuous even at higher nanoparticle loadings. The more homogeneous distribution of elements in CMT films confirms their superior compatibility with both ZnO/CuO nanoparticles and plant extracts, supporting the FESEM observations that CMT forms a more stable and structurally coherent matrix compared to TG. These results highlight the ability of CMT to better stabilize and disperse inorganic and organic additives, which is expected to contribute to the improved mechanical, and barrier properties observed in CMT-based nanocomposite films.

### 3.4. Mechanical properties of films

Properties of the nanocomposite films were evaluated using a universal testing machine (Universal Testing Machine, SANTAM, STD Series, Iran) equipped with a 6 N load cell. The tests were conducted at room temperature with a crosshead speed of 10 mm/min, following the ISO 527 standard for thin polymeric films. Prior to testing, the samples—with an approximate thickness of 100 µm—were cut into strips with dimensions of 10 mm × 60 mm and conditioned at 25 °C for 24 hours to ensure moisture equilibration. In this section, a detailed analysis of the stress–strain behavior of the TG-based (T series) and CMT-based (C series) nanocomposite films are presented. This analysis focuses on tensile strength, elongation at break, and variations in stiffness resulting from the incorporation of metal oxide nanoparticles and plant extracts. Fig. 4A and Fig. 4B show the results of the tensile test. The tensile stress–strain curves of the TG-based (Fig. 4A) and CMT-based (Fig. 4B) nanocomposite films reveal significant differences in their mechanical performance as a function of formulation. In both sets, the incorporation of metal oxide nanoparticles and plant extracts leads to noticeable improvements in tensile strength, although the extent of enhancement varies among samples. For the TG-based films (T series), the neat sample (T) shows the highest elongation at break, indicating a more flexible behavior. Upon the addition of nanoparticles and extracts (T1–T8), the curves shift toward higher stress values, accompanied by a reduction in strain, suggesting that reinforcement increases stiffness but decreases flexibility. Among these films, samples T3, T7, and T8 exhibit the highest stress values, reflecting an effective interaction between TG chains, nanoparticles, and bioactive compounds, which results in stronger and more rigid structures. For the CMT-based films (C series), a similar trend is observed; however, the mechanical improvement is more pronounced compared to the TG series. The neat film (C) displays moderate strength with relatively high strain, while the modified C1–C8 films show significant increases in tensile strength due to the enhanced compatibility provided by carboxymethyl functional groups [39, 40]. Samples C4 and C7 demonstrate the highest tensile strength, confirming that CMT provides a more stable and interconnected network capable of efficient nanoparticle dispersion and stronger hydrogen bonding [41, 42]. Overall, the results show that CMT-based nanocomposites generally outperform TG-based ones in terms of mechanical strength, likely due to their higher branching degree, greater density of carboxymethyl groups, and superior interfacial interactions with the incorporated nanoparticles and plant extracts [43, 44].

### 3.5. Wettability of films

The static contact angle analysis was performed to evaluate the surface wettability of the TG-based (T series) and CMT-based (C series) nanocomposite films. The static contact angle of the films was measured using a Contact Angle Goniometer (CAG20, Jikan, Iran). For each film, measurements were recorded at a minimum of three different surface points, and the mean value was reported as the final contact angle. Statistical analysis was performed using one-way ANOVA, followed by Tukey's post hoc test to identify significant pairwise differences at a 95% confidence level ($p < 0.05$). All data are presented as mean ± standard deviation (SD).

The contact angle measurements (Fig. 4C and 4D) revealed that the surface wettability of the nanocomposite films is strongly influenced by the combined effects of the polymer matrix (TG or CMT), the type of plant extract (cinnamon or clove), and the type and concentration of metal oxide nanoparticles (ZnO or CuO at 3% and 5%).

Overall, CMT-based films exhibited lower contact angles compared to TG-based films, indicating higher hydrophilicity and greater surface energy. In both polymer matrices, samples containing clove extract (samples 3, 4, 7, 8) showed the lowest contact angles due to the presence of polar phenolic groups [45], resulting in enhanced surface hydrophilicity. Conversely, films containing cinnamon extract (samples 1, 2, 5, 6) presented higher contact angles, reflecting a more hydrophobic surface character [46]. The incorporation of nanoparticles further modified the surface behavior. ZnO nanoparticles generally decreased the contact angle and enhanced wettability owing to their semi-polar nature [47, 48],

while CuO nanoparticles—particularly at 5 wt%—in combination with cinnamon extract increased the contact angle, thereby promoting surface hydrophobicity [49, 50]. Increasing nanoparticle content from 3% to 5% amplified these trends and caused notable shifts in surface energy. According to the statistical analysis (one-way ANOVA followed by Tukey's test), several of these variations were statistically significant ($p < 0.05$), confirming that molecular interactions and structural modifications play a key role in determining the surface properties of the films. These findings emphasize the importance of the synergistic selection of extract type and nanoparticle characteristics in engineering active food-packaging films. Based on surface wettability and contact angle behavior, the films can be matched to different food-packaging needs: Films with higher contact angles (more hydrophobic), especially those containing *cinnamon extract + CuO*, are suitable for dry foods, snacks, spices, and moisture-sensitive products, as their lower surface energy provides better moisture barrier performance. Films with moderate contact angles, such as many TG-based samples and certain ZnO-containing films, are appropriate for general food-packaging applications, offering a balanced combination of flexibility, barrier properties, and bioactivity.

Films with low contact angles (more hydrophilic), particularly *CMT + ZnO + clove extract* formulations, are ideal for fresh produce, fruits, vegetables, high-respiration foods, and edible coatings, where controlled moisture exchange is necessary to prevent condensation and maintain freshness. This classification demonstrates that the combined selection of extract type and nanoparticle characteristics can effectively tailor films for specific food-packaging applications.

Due to the high moisture sensitivity and mold susceptibility of raw pistachios, the most suitable films for their packaging are those with higher contact angles and greater hydrophobicity. Among the tested formulations, the films containing cinnamon extract combined with CuO nanoparticles (e.g., T5–T6 and C5–C6) are the most effective, as they provide improved moisture barrier performance and offer strong antibacterial activity (See section 3.6), thereby enhancing the shelf life of raw pistachios.

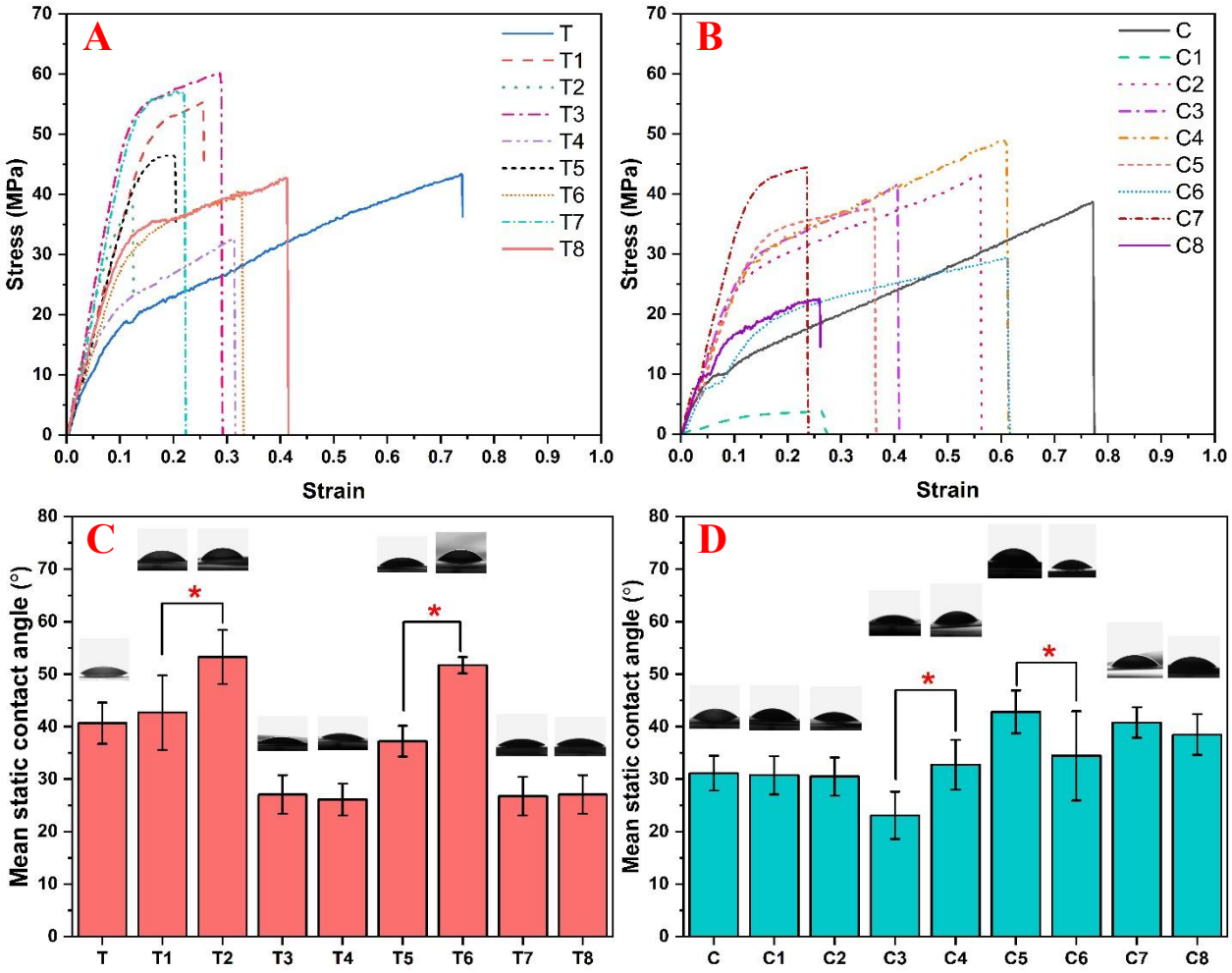


**Figure 4.** Tensile strength and contact angle of neat and nanocomposite films. (A) Tensile strength of TG-based and (B) CMT-based films. (C) Mean static contact angles (°) of TG-based (T–T8) and (D) CMT-based (C–C8) films. Data are presented as mean ± standard deviation (n = 3). Asterisks (*) indicate statistically significant differences ($p < 0.05$) between the indicated groups. Representative contact angle images for each sample are displayed on the corresponding bars

10.57647/jnsc.2026.1602.10

### 3.6. Determining the transparency of films

The optical clarity of the TG- and CMT-based films was evaluated using UV–Vis spectroscopy (Lambda 25, PerkinElmer, USA) at 600 nm. In accordance with commonly used analytical methods for biopolymer films (ASTM D1746-92), the transparency index was calculated using

$$Transparency = \%T = 10^{(2-A)}$$

where $\%T$ is the percent transmittance of light and $A$ is the absorbance of light. And opacity was calculated using the following equation:

$$Opacity = \frac{A_{600}}{x}$$

where $A_{600}$ is the absorbance at 600 nm and x is the film thickness (0.1 mm) [51]. It is important to note that in this definition, higher values represent higher absorbance and therefore greater opacity, whereas lower values indicate greater transparency and higher light transmittance. The results (Table 2) revealed a clear difference between the two polymeric systems. TG-based films exhibited significantly lower opacity index values (mean 2.97 ± 0.97 $mm^{-1}$) compared to CMT-based films (mean 7.56 ± 2.52 $mm^{-1}$), indicating that TG films are substantially more transparent than their CMT counterparts. The higher opacity index of the CMT films suggests greater light absorption and scattering, leading to reduced optical clarity.

The observed difference can be attributed to structural variations between the two gums. Carboxymethylation increases the density of negatively charged groups in CMT, which may enhance water affinity [52], introduce heterogeneity into the polymeric network [53], and promote light scattering [54].

In contrast, TG generally forms more uniform matrices, and its water-soluble fraction (tragacanthin) is known to generate clearer solutions, contributing to the higher transparency of TG films [55]. Overall, these findings demonstrate that TG-based films possess superior optical transparency compared to CMT-based films, making them more suitable for applications such as biodegradable packaging and coating films where higher light transmittance is desirable.

**Table 2.** Transparency and opacity values of films based on TG (T series) and CMT (C series) at a wavelength of 600 nm (film thickness=0.1 mm)

| Sample | $A_{600}$ (Absorbance) | $T = 10^{-A}$ | T (at 600 nm) % | Opacity Index ($mm^{-1}$) |
|---|---|---|---|---|
| T | 0.12726 | 0.74600 | 74.60% | 1.2726 |
| T1 | 0.28889 | 0.51417 | 51.42% | 2.8889 |
| T2 | 0.31647 | 0.48254 | 48.25% | 3.1647 |
| T3 | 0.24211 | 0.57265 | 57.27% | 2.4211 |
| T4 | 0.18777 | 0.64898 | 64.90% | 1.8777 |
| T5 | 0.41883 | 0.38122 | 38.12% | 4.1883 |
| T6 | 0.40023 | 0.39790 | 39.79% | 4.0023 |
| T7 | 0.34869 | 0.44803 | 44.80% | 3.4869 |
| T8 | 0.34440 | 0.45248 | 45.25% | 3.4440 |
| C | 0.37617 | 0.42057 | 42.057% | 3.7617 |
| C1 | 0.71788 | 0.19148 | 19.148% | 7.1788 |
| C2 | 0.68319 | 0.20740 | 20.740% | 6.8319 |
| C3 | 0.55536 | 0.27838 | 27.838% | 5.5536 |
| C4 | 0.52586 | 0.29795 | 29.795% | 5.2586 |
| C5 | 1.14941 | 0.70890 | 70.890% | 11.4941 |
| C6 | 1.03137 | 0.09303 | 9.303% | 10.3137 |
| C7 | 0.92328 | 0.11932 | 11.932% | 9.2328 |
| C8 | 0.83759 | 0.14535 | 14.535% | 8.3759 |

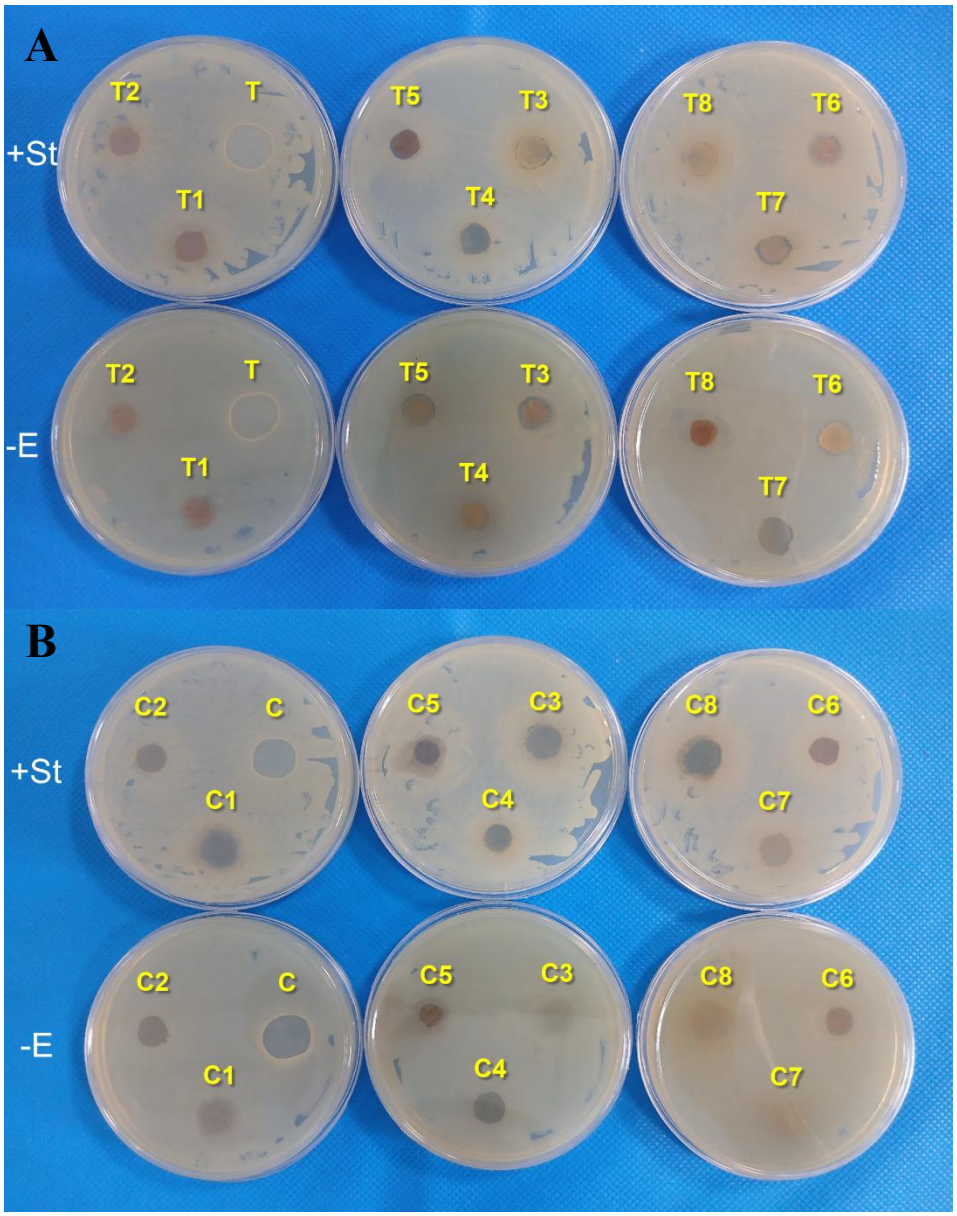


**Figure 5.** Images of the antibacterial test on various (A) TG- and (B) CMT-based neat and nanocomposite films

**Table 3.** Inhibition zone diameter (mm) for TG- (T series) and CMT-based (C series) nanocomposite films

| Sample | *Escherichia coli (-E)* | *Staphylococcus aureus (+St)* | Sample | *Escherichia coli (-E)* | *Staphylococcus aureus (+St)* |
|---|---|---|---|---|---|
| T | 0 | 0 | C | 0 | 0 |
| T1 | 10 | 0 | C1 | 0 | 12 |
| T2 | 10 | 0 | C2 | 0 | 0 |
| T3 | 11 | 11 | C3 | 0 | 12 |
| T4 | 0 | 0 | C4 | 0 | 0 |
| T5 | 9 | 10 | C5 | 0 | 9 |
| T6 | 11 | 10 | C6 | 0 | 0 |
| T7 | 0 | 10 | C7 | 0 | 0 |
| T8 | 10 | 11 | C8 | 0 | 0 |

10.57647/jnsc.2026.1602.10

### 3.7. Antibacterial studies of films

The antibacterial properties of the synthesized films were evaluated through antimicrobial assays against two representative bacterial strains, Escherichia coli (-E) and Staphylococcus aureus (+St) (Fig. 5). These tests were conducted to assess the films' ability to inhibit microbial growth and to enhance the safety and shelf life of food products. The following results indicate that the incorporation of nanoparticles and plant extracts plays a significant role in improving the antibacterial activity of the films.

The antibacterial assay results (Table 3) of TG- and CMT-based films indicate that the presence of active components, including nanoparticles and plant extracts, significantly inhibits bacterial growth. For TG-based films, samples T1, T2, and T3 showed inhibition zones of 10–11 mm against Escherichia coli, whereas antibacterial activity against Staphylococcus aureus was mainly observed in T3, T5-T6. Similarly, among the CMT-based films, samples C1 and C3 exhibited the highest antibacterial activity against Staphylococcus aureus, while none of the samples inhibited Escherichia coli. These results suggest that the specific combination of nanoparticles and plant extracts can exert selective effects on different bacterial species, providing notable antibacterial performance for food packaging applications.

For comparison, standard antibiotics tested under CLSI-recommended disk diffusion conditions typically exhibit inhibition zones for susceptible strains of foodborne bacteria of ≥17 mm for ampicillin and ≥15 mm for gentamicin at the indicated disc concentrations. These values serve as benchmark references for antimicrobial efficacy [56].

In contrast, the inhibition zones observed for the developed nanocomposite films are smaller but still significant, reflecting their role as antimicrobial packaging materials rather than therapeutic agents. The sustained release of bioactive compounds and metal ions from the films contributes to effective microbial growth suppression on food surfaces over extended storage periods.

In the present study, the antibacterial activity of the composite films was evaluated using the agar diffusion (zone of inhibition) method, which is a widely accepted qualitative–semiquantitative approach for assessing the antimicrobial performance of solid polymeric materials and food packaging films [57]. This method provides a direct and reproducible indication of bacterial growth suppression through the formation of clear inhibition zones around the samples, resulting from the diffusion of active antimicrobial species from the film matrix into the surrounding agar medium. While quantitative techniques such as bacterial colony counting or fluorescence-based live/dead staining can offer additional insights into bacterial viability, they are not essential for confirming comparative antibacterial performance in applied food packaging studies [58]. Therefore, the antibacterial evaluation in this work focuses on comparative inhibition efficiency among different film formulations, which is sufficient to demonstrate the antimicrobial contribution of ZnO and CuO nanoparticles within the biopolymer matrix.

### 3.8. Antioxidant studies of films

In this study, the antioxidant activity of the nanocomposite films based on TG and CMT was evaluated using the DPPH radical inhibition assay following Brand-Williams et al. [59] with minor modifications. A 25 ppm DPPH solution was first prepared, and 0.01 g of each film sample was immersed in 1 mL of this solution (Fig. 6A and Fig. 6B). The characteristic deep purple color of the DPPH radical is clearly visible, indicating that no radical inhibition has occurred at this initial stage (0 h). The samples were kept in the dark at room temperature for 24 hours to allow the antioxidant compounds within the films to interact with the DPPH radicals (24 h). The observable discoloration of the DPPH medium surrounding the films indicates radical inhibition activity, with the extent of color fading corresponding to the antioxidant capacity of each film formulation. After incubation, the supernatant was collected, and its absorbance was measured at 517 nm. The radical inhibition activity (percent inhibition) was calculated using the following equation:

$$\%\ Inhibition = \frac{A_{control} - A_{sample}}{A_{control}} \times 100$$

where $A_{control}$ is the absorbance of the DPPH solution without sample and $A_{sample}$ is the absorbance with the tested sample. To quantify the antioxidant capacity in terms of a known standard, an ascorbic acid (AA) calibration curve was generated [59]. Ascorbic acid solutions with concentrations of 5, 10, 25, 50, and 100 mg/mL were prepared, and 0.5 mL of each solution was mixed with 0.5 mL of DPPH. After 30 minutes of incubation in the dark, absorbance was recorded at 517 nm, and inhibition percentages were calculated. A calibration curve (inhibition percentage vs. ascorbic acid concentration) was then constructed (Fig. 6C), and the obtained regression equation was used to determine the ascorbic acid equivalents (AAE) of the film samples. Standard equation:

$$38.6562 + 0.41715x = y$$
$$\frac{y - 38.6562}{0.41715} = x$$

10.57647/jnsc.2026.1602.10

The results demonstrated that both TG- and CMT-based films exhibited considerable antioxidant activity (Table 4). The inhibition percentages for the TG samples ranged from 30.8% to 71.3%, whereas the CMT samples ranged from 28.3% to 70.7%, indicating the ability of these films to inhibit free radicals. Variations among samples can be attributed to differences in the gum matrix, polymer network structure, and interactions between nanoparticles and plant extracts [60].

Based on the standard curve equation, AAE values were calculated. It should be noted that due to the mathematical nature of this parameter, some values fell below zero; since negative antioxidant equivalents have no physical meaning, such values were reported as zero, according to standard scientific practice. This approach is consistent with the concept of estimating capacity at zero concentration [61] and aligns with best practices in analytical antioxidant assays to avoid misinterpretation of biologically meaningless negative values [62].

Overall, the findings indicate that the incorporation of ZnO or CuO nanoparticles together with plant extracts such as cinnamon or clove significantly enhances the antioxidant capability of the films. This improvement highlights their potential application as bioactive food-packaging materials capable of inhibiting oxidation and extending shelf life.

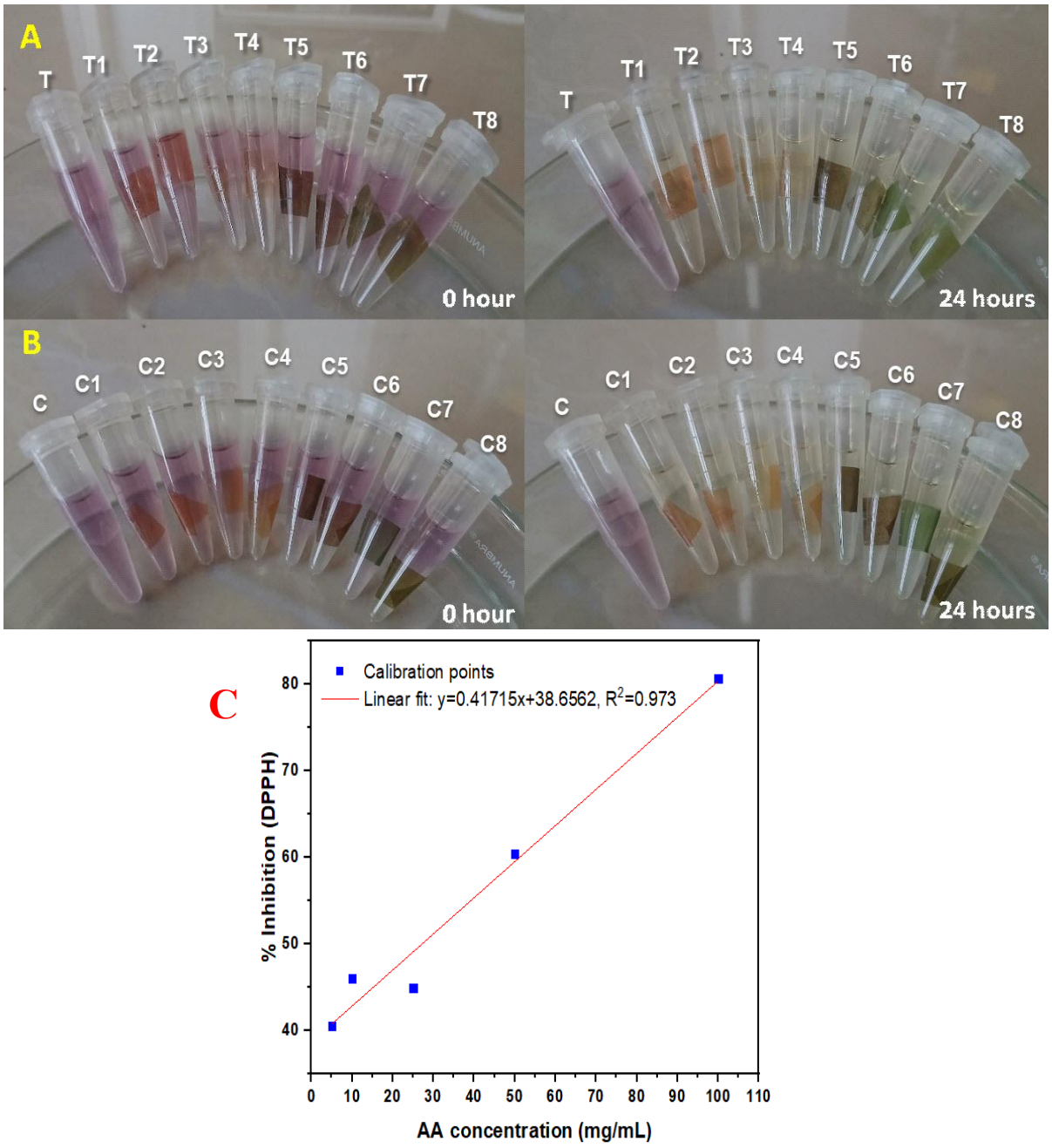


**Figure 6.** Visual appearance of (A) TG- and (B) CMT-based films immediately after immersion (0 h) and after 24 h of incubation in DPPH solution (24 h). **(C)** Calibration curve of ascorbic acid (AA) used for quantifying antioxidant capacity. The linear relationship between absorbance and AA concentration was used to calculate the ascorbic acid equivalent (AAE) values of the samples

10.57647/jnsc.2026.1602.10

**Table 4.** Antioxidant test results of TG- (T series) and CMT- (C series) based films

| Sample | Inhibition (%) | Ascorbic Acid Equivalent (AAE), mg/mL | Sample | Inhibition (%) | Ascorbic Acid Equivalent (AAE), mg/mL |
|---|---|---|---|---|---|
| T | 30.82 | 0* | C | 28.30 | 0* |
| T1 | 62.95 | 58.24 | C1 | 70.36 | 76.00 |
| T2 | 63.27 | 59.00 | C2 | 66.48 | 66.70 |
| T3 | 64.65 | 62.31 | C3 | 70.46 | 76.24 |
| T4 | 71.31 | 78.28 | C4 | 67.56 | 69.29 |
| T5 | 62.14 | 56.30 | C5 | 67.56 | 69.29 |
| T6 | 66.17 | 65.96 | C6 | 64.22 | 61.28 |
| T7 | 65.86 | 65.21 | C7 | 70.73 | 76.89 |
| T8 | 66.08 | 65.74 | C8 | 50.93 | 29.42 |

* In cases where the absorbance of the sample exceeded that of the control, the calculated inhibition percentage yielded a negative value. Such negative values were set to zero, as recommended in DPPH assay methodology, because negative inhibition activity has no physiological relevance

### 3.9. Biodegradability studies of films

To evaluate biodegradability, film samples measuring 2 × 2 cm were cut and buried in potting soil at a depth of 2–3 cm. The soil was regularly watered over a period of 100 days to maintain moisture and provide suitable conditions for degradation. After 100 days, the samples were retrieved from the soil, and photographs were taken to assess visual changes and the extent of degradation

The biodegradation results (Fig. 7) reveal significant degradation in both TG-based and CMT-based films after 100 days of soil burial, though the extent and pattern of decomposition varied among the samples.

In the TG-based films (T series), the neat film (T) and all modified samples (T1–T8) were highly fragmented after 100 days, indicating high biodegradability of TG-based films. The presence of ZnO or CuO nanoparticles and plant extracts did not hinder the degradation process; in some cases, the organic nature of the extracts may have even enhanced microbial activity and accelerated breakdown [63]. In the CMT series, an important observation is that samples C2, C3, C7, and C8 were completely decomposed, leaving no visible residues in the 100-day image. This suggests that the combination of specific fillers and clove extract in these films significantly increased biodegradability, likely due to the microbial stimulatory effects of phenolic compounds [13]. Conversely, samples such as C1, C4, C5, and C6 retained larger fragments, indicating greater structural stability, which aligns with the more compact, ionically cross-linked and cohesive network of CMT, typically known to slow water penetration and microbial enzymatic activity [64]. Overall, TG films exhibit the most uniform biodegradation rate. CMT films show filler- and extract-dependent behavior, with some samples fully degraded (C2, C3, C7, C8) and others displaying moderate stability. These findings suggest that TG films are ideal for short-term, fully biodegradable packaging, while selected CMT films (C1, C4, C5, C6) are better suited for applications requiring longer-lasting structural integrity.

The apparent contradiction between lower contact angles (higher surface hydrophilicity), reduced bulk moisture absorption, and enhanced biodegradation for certain CMT films can be reconciled by recognizing the different scales probed by the measurements. Contact angle reflects surface polarity and promotes microbial adhesion [65], whereas moisture absorption measures bulk water diffusion. A denser, low-free-volume CMT network can limit bulk water absorption, while its polar surface (carboxymethyl groups) increases microbial attachment and enzyme adsorption. Once colonized, microbes secrete enzymes that locally depolymerize the surface and progressively penetrate the film. Additionally, plant extracts and dissolved ions can stimulate microbial activity, and microstructural defects from nanoparticle distribution can create preferential degradation sites. Collectively, these factors explain why some CMT films exhibit lower moisture absorption yet faster biological degradation [13]. In addition to biodegradability, the biocompatibility and safety of the developed composite films are critical considerations for food packaging applications. The films in this study are composed exclusively of naturally derived polysaccharides (tragacanth gum and carboxymethyl tragacanth gum) and metal oxide nanoparticles (ZnO and CuO), all of which have been extensively reported as safe and suitable for food-related applications when used within controlled concentrations.

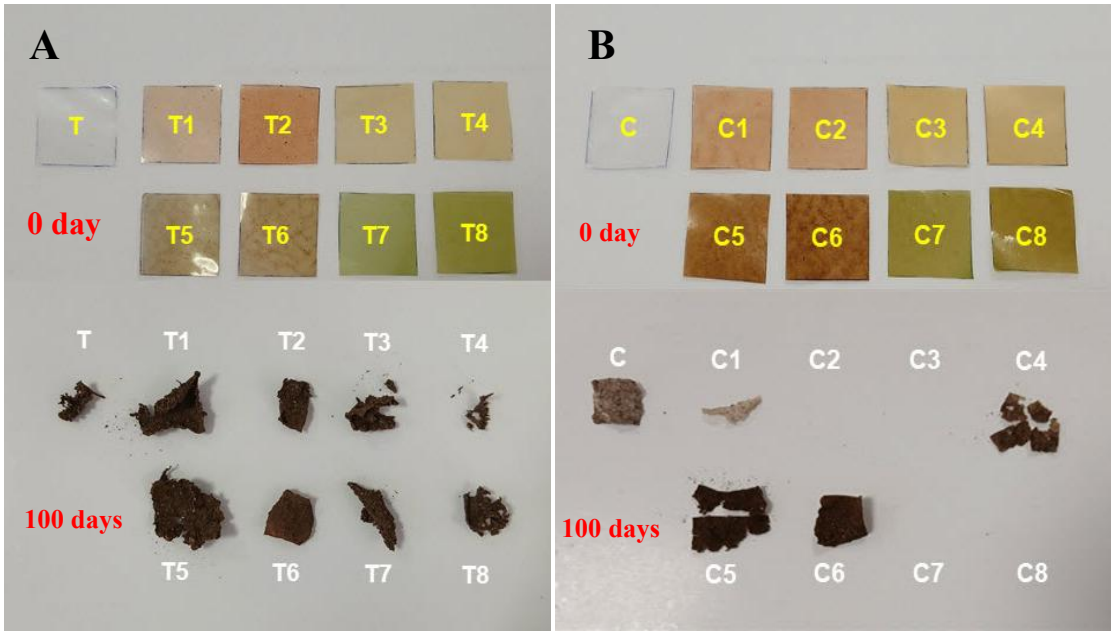


**Figure 7.** Biodegradability test images of (A) TG- (T series) and (B) CMT- (C series) based films

In addition to biodegradability, the biocompatibility and safety of the developed composite films are critical considerations for food packaging applications. The films in this study are composed exclusively of naturally derived polysaccharides (tragacanth gum and carboxymethyl tragacanth gum) and metal oxide nanoparticles (ZnO and CuO), all of which have been extensively reported as safe and suitable for food-related applications when used within controlled concentrations. Tragacanth-based polymers are biodegradable, non-toxic, and generally recognized as safe (GRAS), with long-standing use in food and pharmaceutical products [66, 67]. ZnO and CuO nanoparticles have also been widely employed in antimicrobial food packaging systems, and their safety profiles are well documented in the literature [68, 69]. Importantly, SEM, FTIR, and XRD analyses confirm that ZnO and CuO nanoparticles are immobilized within the polymer matrix rather than existing as free particles. Such immobilization significantly reduces potential cytotoxicity by limiting direct biological exposure and uncontrolled ion release [70, 71]. Therefore, based on material composition, structural immobilization, degradation behavior, and extensive literature evidence, the developed composite films demonstrate a favorable biocompatibility profile suitable for food packaging applications [72, 73].

### 3.10. Determination of moisture absorption

The moisture absorption test was conducted in accordance with standard procedures for evaluating the humidity response of biopolymer-based films, aiming to determine their hydrophilic stability and sensitivity to environmental moisture key performance factors in food packaging applications.

Moisture absorption was determined according to ASTM E104-02 using a saturated NaCl solution (75 ± 2% RH at 25 °C). Before placing the film samples in the desiccator, each specimen was initially weighed. A 1 cm layer of saturated NaCl solution had been introduced into the desiccator approximately 2 h prior to testing, and the samples were placed on a mesh stand above the solution. The films were reweighed at predetermined time intervals of 24, 48, and 72 h (extended to 120 h in this study) (Fig. 8A). The moisture absorption percentage was then calculated using the following equation:

$$\text{Moisture absorption (\%)} = \frac{W_t - W_0}{W_0} \times 100$$

where $W_0$ is the initial dry weight and $W_t$ is the weight at each time point (according to ASTM E104 standard). Based on the results of tensile and antibacterial tests, samples T3 and C3 were selected as the optimal formulations for subsequent moisture absorption and gas permeability evaluations (see Section 3.11). These samples exhibited a favorable balance between tensile strength and elongation at break, along with enhanced antibacterial performance, while maintaining a homogeneous morphology and uniform nanoparticle dispersion as observed in FESEM analyses. The moisture absorption results (Fig. 8B and Fig. 8C) for samples T3 and C3, each evaluated with five replicates, indicate a similar increasing trend in moisture uptake over the 120-hour period. Sample T3 exhibited a higher initial moisture absorption (approximately 21% at 24 hours), gradually rising to 24.59% at 120 hours. This moderate increase suggests that the presence of metal oxide nanoparticles

and clove extract enhances the interaction of the TG-based matrix with environmental humidity, leading to slightly greater water retention capacity. Conversely, sample C3 consistently showed lower moisture absorption across all time points (starting at 19.62% and increasing to 22.87% at 120 hours). This behavior can be attributed to the more branched, structured, and compact nature of the CMT polymer network, which generally reduces water permeability and creates a more effective barrier against moisture penetration [74]. Overall, the comparison shows that C3 demonstrates lower and more stable moisture absorption, making it more suitable for packaging food products sensitive to humidity. Meanwhile, T3 exhibits slightly higher moisture uptake, which may be beneficial in applications where gradual moisture regulation is desirable.

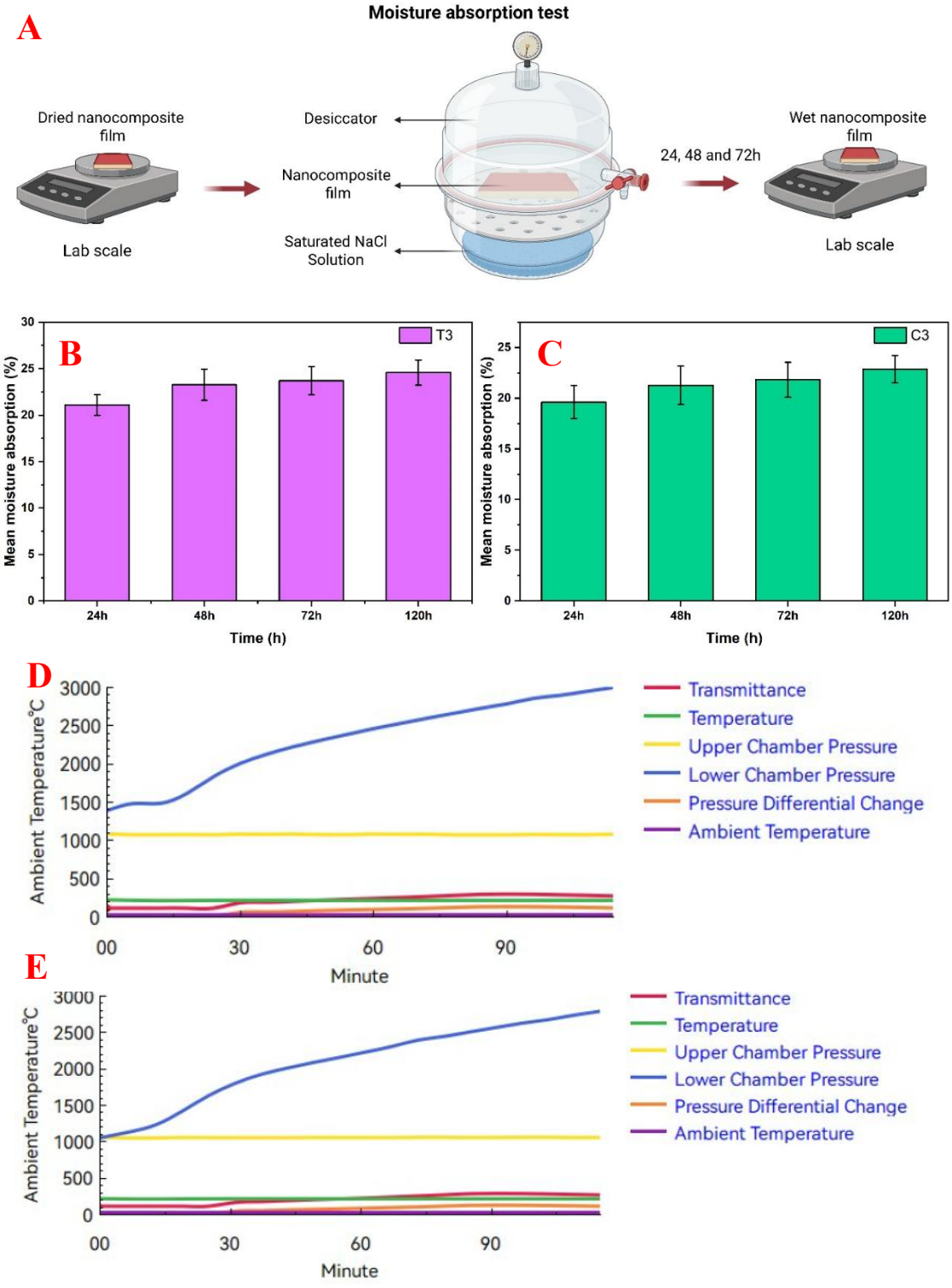


**Figure 8.** Results of moisture absorption and gas permeability tests for optimized samples (T3 and C3). (A) Moisture absorption test schematic. Moisture absorption results for (B) T3 and (C) C3; bar chart showing mean ± SD (n = 5). Gas permeability result for (D) T3 and (E) C3

10.57647/jnsc.2026.1602.10

### 3.11. Gas permeability measurement

The oxygen permeability of samples T3 and C3 was evaluated using a gas permeability analyzer according to ASTM D1434 at 23 °C under an oxygen atmosphere. Both samples were tested with a constant effective area of 50.24 $cm^2$. The thicknesses of T3 and C3 were measured to be 78 µm and 70 µm, respectively. Sample C3 exhibited a lower oxygen transmission rate (26.80 $cm^3/m^2 \cdot 24\ h \cdot 0.1$ MPa) compared to T3 (27.53 $cm^3/m^2 \cdot 24\ h \cdot 0.1$ MPa), despite its lower thickness (Figs. 8D and 8E). This result indicates an intrinsically improved oxygen barrier performance for C3.

The diffusion coefficient of oxygen in C3 ($D=8.17 \times 10^{-6}$ $cm^2/s$) was significantly higher than that of T3 ($D=2.26 \times 10^{-8}$ $cm^2/s$), while the oxygen solubility coefficient showed an opposite trend, with C3 exhibiting a markedly lower solubility ($S(C3)=2.66 \times 10^{-10}$ $cm^3/cm^2.cm.Pa$, and $S(T3) =1.1 \times 10^{-7}$ $cm^3/cm^2.cm.Pa$). Since gas permeability is governed by the product of diffusion and solubility ($P = D \times S$), the reduced oxygen solubility in C3 outweighs the effect of its higher diffusion coefficient, resulting in an overall lower oxygen transmission rate. In contrast, the higher lag time observed for T3 (449 s compared to 1 s for C3) suggests a denser polymer network that delays initial oxygen permeation; however, the higher oxygen solubility within its matrix ultimately leads to increased steady-state permeation.

These findings are consistent with morphological observations from FESEM analysis, where a more uniform and compact microstructure with fewer microcracks was observed for C3, facilitating reduced gas solubility. Additionally, the improved barrier behavior of C3 correlates well with its lower contact angle and stronger intermolecular interactions, which likely decrease the free volume within the polymer matrix. Overall, the enhanced oxygen barrier performance of C3 highlights its potential suitability for oxygen-sensitive food packaging applications, where reduced oxygen transmission is critical for prolonging shelf life and preventing oxidative degradation.

In addition to the quantitative permeability parameters, the real-time evolution of transmittance, pressure, and temperature profiles shown in Figs. 8D and 8E provides further insight into the gas transport behavior of samples T3 and C3. For both samples, a gradual increase in oxygen transmittance was observed with time until a quasi-steady state was reached, indicating the establishment of stable permeation conditions. The delayed rise in transmittance for sample T3 is consistent with its longer lag time, reflecting a more resistant initial diffusion stage through the polymer matrix. In contrast, sample C3 exhibited a more rapid onset of transmittance, in agreement with its significantly shorter lag time.

The pressure profiles reveal a continuous increase in the lower chamber pressure while the upper chamber pressure remained nearly constant throughout the experiment, confirming proper sealing and stable operating conditions of the permeability cell. Notably, the slope of the lower chamber pressure increase was slightly lower for C3 compared to T3, which is consistent with its reduced oxygen transmission rate at steady state. This observation further supports the conclusion that, despite faster initial diffusion, the overall oxygen transport through C3 is effectively restricted.

Moreover, the temperature profiles remained relatively stable during the measurements, with only minor fluctuations around the set point, indicating that thermal effects did not significantly influence the permeability results. The reproducible and smooth trends observed in both figures confirm the reliability of the experimental data and the intrinsic nature of the differences between T3 and C3. Overall, the time-dependent permeation behavior depicted in Figs. 8D and 8E corroborates the quantitative permeability analysis and highlights the superior oxygen barrier efficiency of sample C3.

## 4. Practical application: Preservation performance of the developed edible films on raw pistachios

The practical applicability of the developed edible films was evaluated through their use as active packaging materials for raw pistachios, a high-value nut highly susceptible to microbial contamination, oxidative degradation, and quality deterioration during storage. The edible films were formulated based on tragacanth gum (TG) and carboxymethyl tragacanth (CMT), reinforced with biogenic zinc oxide (ZnO) or copper oxide (CuO) nanoparticles and enriched with natural plant extracts, namely clove or cinnamon, to impart antimicrobial and antioxidant functionalities. This application study was designed to assess the real-world preservation potential of the films beyond laboratory-scale characterization.

Raw pistachios were uniformly coated with the developed edible films and stored under ambient conditions to simulate typical market and household storage environments. For comparison, pistachios packaged in conventional commercial plastic bags commonly used in the market were considered as control samples. During the storage period, both coated and control pistachios were visually monitored to evaluate their apparent quality, including surface appearance, discoloration, and the presence of visible microbial spoilage. No quantitative microbiological or physicochemical analyses were performed, and the assessment was limited to visual observations.

10.57647/jnsc.2026.1602.10


**Figure 9.** Packaging of raw pistachios using conventional plastic films and TG/CMT-based edible films containing biogenic nanoparticles and plant extracts. The active edible films significantly improved the preservation quality and extended the shelf life of pistachios during storage

The results demonstrated that pistachios coated with the functionalized edible films exhibited noticeably improved visual stability compared to the control samples packaged in conventional plastic bags. While the control pistachios showed visible signs of quality deterioration and microbial spoilage during storage, the pistachios packaged with the TG- and CMT-based edible films remained free from observable spoilage for up to 12 days under ambient conditions (Fig. 9). This improvement in apparent shelf life suggests that the developed edible films provide enhanced protective effects compared to conventional plastic packaging.

The improved preservation performance can be attributed to several synergistic mechanisms inherent to

the film formulation. First, the reduced oxygen permeability of the TG- and especially CMT-based films, as confirmed by gas permeability measurements, limited oxygen diffusion to the pistachio surface, thereby slowing oxidative reactions responsible for rancidity and quality loss. Second, the enhanced mechanical integrity of the films ensured sufficient coating stability and surface coverage during storage, preventing film cracking or detachment that could expose the pistachios to environmental contaminants.

Moreover, the incorporation of biogenic ZnO or CuO nanoparticles imparted strong antimicrobial activity to the films. These nanoparticles are known to inhibit the growth of a wide range of microorganisms through mechanisms such as the generation of reactive oxygen species, disruption of microbial cell membranes, and interference with essential cellular processes.

In parallel, the presence of clove or cinnamon extracts further enhanced the antimicrobial efficacy due to their bioactive compounds, such as eugenol and cinnamaldehyde, which exhibit well-documented antimicrobial and antioxidant properties. The combination of metal oxide nanoparticles and plant extracts within the biopolymer matrix resulted in a synergistic effect, providing sustained antimicrobial protection at the food–film interface.

Additionally, the hydrophilic nature and compact network structure of the TG- and CMT-based films contributed to controlled moisture interactions, reducing surface condensation and creating less favorable conditions for microbial proliferation. The stronger intermolecular interactions and denser network structure observed in CMT-based films further enhanced this effect, explaining their superior preservation performance in comparison to TG-based counterparts.

Importantly, the edible and bio-based nature of the developed films addresses increasing consumer and industrial demands for sustainable and environmentally friendly food packaging solutions. The use of natural polysaccharides, green-synthesized nanoparticles, and plant-derived extracts ensures that the films are not only effective but also aligned with clean-label and eco-conscious packaging trends. The simplicity of the coating process further supports the feasibility of scaling up this technology for commercial applications.

Overall, the application study on raw pistachios demonstrates that the developed TG- and CMT-based edible films function as efficient active packaging systems capable of significantly extending shelf life while preserving product quality under ambient storage conditions. These findings underscore the strong potential of the formulated films for practical use in the preservation of raw pistachios and other high-value nuts and dried food products, offering a promising strategy for reducing post-harvest losses and enhancing food safety through sustainable packaging technologies.

## 5. Future prospects

Beyond pistachio packaging, the developed TG- and CMT-based nanocomposite films show strong potential for application in a wide range of food packaging systems, including dried fruits, nuts, bakery products, and oxygen- or moisture-sensitive foods, where balanced mechanical strength and barrier performance are critical. From an industrial perspective, future studies should focus on scale-up challenges such as process reproducibility, cost-effectiveness of nanoparticle incorporation, and compatibility with conventional film-forming and coating technologies. In addition, although the current results demonstrate promising performance, comprehensive in vivo toxicity and long-term migration studies will be essential to fully assess the safety of these nanocomposite films and support their regulatory approval and commercial implementation.

## 6. Conclusions

This study demonstrates that the incorporation of natural polysaccharides, namely TG and CMT, in combination with biogenic metal oxide nanoparticles (ZnO or CuO) and plant-derived extracts (cinnamon or clove), effectively enhances both the mechanical and oxygen barrier properties of PVA-based bio-nanocomposite films. Specifically, the tensile strength increased from 38.84 MPa in the neat CMT-based film to 41.69 MPa in its optimized formulation, whereas the TG-based films exhibited an increase from 43.46 MPa in the neat film to 60.31 MPa upon optimization. Although some TG-based films exhibit higher tensile strength (44% higher than the corresponding CMT-based films), CMT-based films demonstrate a more favorable balance between strength and elongation, resulting in improved toughness and mechanical stability, which are critical for flexible food packaging applications. Comparative analysis of the obtained results revealed that CMT-based films consistently outperformed their TG-based counterparts across multiple characterization techniques. FESEM observations confirmed that CMT-containing films exhibited a more compact, and homogeneous microstructure with improved nanoparticle dispersion, which is essential for efficient stress transfer and the suppression of gas transport pathways. Surface wettability measurements showed a lower contact angle for CMT-based films, (23.1° for optimized CMT-based films compared to 27.6° for optimized TG-based films) indicating enhanced intermolecular interactions and reduced free volume within the polymer matrix. Oxygen

10.57647/jnsc.2026.1602.10

permeability analysis demonstrated that the optimized CMT-based film (C3) achieved a lower oxygen transmission rate (26.80 $cm^3/m^2 \cdot 24\ h \cdot 0.1\ MPa$) than the corresponding optimized TG-based film (T3) (27.53 $cm^3/m^2 \cdot 24\ h \cdot 0.1\ MPa$), despite its reduced thickness (70 µm versus 78 µm). Detailed evaluation of diffusion and solubility coefficients revealed that the improved barrier performance of C3 was predominantly governed by decreased oxygen solubility ($S(C3)=2.66 \times 10^{-10}$ $cm^3/cm^2.cm.Pa$) rather than diffusion resistance. Overall, the convergence of structural, surface, mechanical, and gas barrier improvements highlights the superiority of CMT over TG as a reinforcing polysaccharide. Quantitatively, CMT-based films exhibited simultaneous improvements in tensile strength, surface wettability, and oxygen barrier performance, while maintaining suitable film integrity and thickness. The developed CMT-based nanocomposite films therefore represent promising candidates for sustainable, high-performance food packaging applications requiring a balanced combination of mechanical durability and effective oxygen barrier functionality.

## Acknowledgment

This work was supported by the Iran National Science Foundation (INSF) under Grant Number 4027939. The study was also supported by Medical and Health Talent Research Initiation Fund Class G (Grant Number KYQD2024-020), The Quzhou Affiliated Hospital of Wenzhou Medical University.

**Statement**
During the preparation of this work, the authors used BioRender to create schematic illustrations, Origin for plotting graphs, histograms, and performing statistical analyses, and AI-assisted tools (such as language editing software) to refine and improve the clarity of the manuscript text.

**Authors Contribution**
**Zohre Jafari Vafa:** Methodology, Investigation, Data curation, Formal analysis, Writing – original draft. **Ehsan Nazarzadeh Zare:** Conceptualization, Writing – review & editing, Validation. **Ali Najafi:** Writing – review & editing. **Taotao Zhao:** Writing – review & editing.

**Data Availability**
The data that support the findings of this study are available from the corresponding author upon reasonable request.

**Conflict of Interest**
The authors declare no conflict of interest.

## References

[1] Islamipour, Z., Zare, E. N., Salimi, F., Ghomi, M. and Makvandi, P. Biodegradable antibacterial and antioxidant nanocomposite films based on dextrin for bioactive food packaging. *J. Nanostruct. Chem.* **12**, 991–1006 (2022).

[2] Zare, E. N., Makvandi, P. and Tay, F. R. Recent progress in the industrial and biomedical applications of tragacanth gum: A review. *Carbohydr. Polym.* **212**, 450–467 (2019).

[3] Tavakolipour, H. Postharvest operations of pistachio nuts. *J. Food Sci. Technol.* **52**, 1124–1130 (2015).

[4] Ozturk, I., Sagdic, O., Yalcin, H., Capar, T. D. and Asyali, M. H. The effects of packaging type on the quality characteristics of fresh raw pistachios (Pistacia vera L.) during the storage. *LWT-Food Sci. Technol.* **65**, 457–463 (2016).

[5] Saeedi, M., Mirdehghan, S. H., Saba, M. K. and Nazoori, F. Strategies to preserve quality and improve storage life of fresh in-hull pistachio: a review. *Postharvest Biol. Technol.* **230**, 113751 (2025).

[6] Gopinath, K., Sathishkumar, G. and Xu, L. An overview of the copper oxide nanofillers integrated in food packaging systems. *Coatings* **14**, 81 (2024).

[7] Mesgari, M., Aalami, A. H., Sathyapalan, T. and Sahebkar, A. A comprehensive review of the development of carbohydrate macromolecules and copper oxide nanocomposite films in food nanopackaging. *Bioinorg. Chem. Appl.* **2022**, 7557825 (2022).

[8] Anugrah, D. S. B., Alexander, H., Pramitasari, R., Hudiyanti, D. and Sagita, C. P. A review of polysaccharide-zinc oxide nanocomposites as safe coating for fruits preservation. *Coatings* **10**, 988 (2020).

[9] Jafarzadeh, S., et al. Green synthesis of nanomaterials for smart biopolymer packaging: challenges and outlooks. *J. Nanostruct. Chem.* **14**, 113–136 (2024).

[10] Xie, Q., Liu, G., Zhang, Y., Yu, J., Wang, Y. and Ma, X. Active edible films with plant extracts: A updated review of their types, preparations, reinforcing properties, and applications in muscle foods packaging and preservation. *Crit. Rev. Food Sci. Nutr.* **63**, 11425–11447 (2023).

[11] Gürler, N. and Ertekin, Ö. Physical and biological characteristics of eco-friendly films added with Cinnamomum zeylanicum extract for packaging materials. *Int. J. Food Sci. Technol.* **59**, 2400–2410 (2024).

[12] Roy, S. and Rhim, J. W. Gelatin/cellulose nanofiber-based functional films added with mushroom-mediated sulfur nanoparticles for active packaging applications. *J. Nanostruct. Chem.* **12**, 979–990 (2022).

[13] Ghani, A., Zare, E. N., Makvandi, P. and Rabiee, N. Antioxidant, antibacterial and biodegradable hydrogel films from carboxymethyl tragacanth gum and clove extract: Potential for wound dressings application. *Carbohydr. Polym. Technol. Appl.* **7**, 100428 (2024).

[14] Janani, N., Zare, E. N., Salimi, F. and Makvandi, P. Antibacterial tragacanth gum-based nanocomposite films carrying ascorbic acid antioxidant for bioactive food packaging. *Carbohydr. Polym.* **247**, 116678 (2020).

[15] Lakshmanan, M. Plant extraction methods. in *Introduction to Basics of Pharmacology and Toxicology: Volume 3: Experimental Pharmacology: Research Methodology and Biostatistics* 773–783 (Springer, 2022).

[16] Alves-Silva, G. F., Santos, L. G., Martins, V. G. and Cortez-

Vega, W. R. Cassava starch films incorporated with clove essential oil and nanoclay as a strategy to increase the shelf life of strawberries. *Int. J. Food Sci. Technol.* **57**, 6690–6698 (2022).

[17] Ahmed, M., Saini, P., Iqbal, U. and Sahu, K. Edible microbial cellulose-based antimicrobial coatings and films containing clove extract. *Food Prod. Process. Nutr.* **6**, 65 (2024).

[18] Azadi, A., Rafieian, F., Sami, M. and Rezaei, A. Fabrication, characterization and antimicrobial activity of chitosan/tragacanth gum/polyvinyl alcohol composite films incorporated with cinnamon essential oil nanoemulsion. *Int. J. Biol. Macromol.* **245**, 125225 (2023).

[19] Luesuwan, S., Naradisorn, M., Shiekh, K. A., Rachtanapun, P. and Tongdeesoontorn, W. Effect of active packaging material fortified with clove essential oil on fungal growth and post-harvest quality changes in table grape during cold storage. *Polymers* **13**, 3445 (2021).

[20] Rizal, S., et al. Cinnamon-nanoparticle-loaded macroalgal nanocomposite film for antibacterial food packaging applications. *Nanomaterials* **13**, 560 (2023).

[21] Gürler, N. and Ertekin, Ö. Physical and biological characteristics of eco-friendly films added with Cinnamomum zeylanicum extract for packaging materials. *Int. J. Food Sci. Technol.* **59**, 2400–2410 (2024).

[22] Saeednia, S., Iranmanesh, P. and Shabani, T. Green Synthesis of Pistachio Skin Extract-Mediated Zinc Oxide Nanoparticles for Photocatalytic Degradation of Organic Dyes. *Inorg. Chem. Res.* **8**, 1–7 (2024).

[23] Murugan, B., et al. Green synthesis of CuO nanoparticles for biological applications. *Inorg. Chem. Commun.* **155**, 111088 (2023).

[24] Gao, Q., Feng, Z., Wang, J., Zhao, F., Li, C. and Ju, J. Application of nano-ZnO in the food preservation industry: antibacterial mechanisms, influencing factors, intelligent packaging, preservation film and safety. *Crit. Rev. Food Sci. Nutr.* **65**, 4327–4353 (2025).

[25] Perumal, M. K. K., Rajasekaran, M. B. S., Renuka, R. R., Samrot, A. V. and Nagarajan, M. Zinc oxide nanoparticles and their nanocomposites as an imperative coating for smart food packaging. *Appl. Food Res.* **2025**, 100849 (2025).

[26] Hamdy, M. S., Chandekar, K. V., Shkir, M., AlFaify, S., Ibrahim, E. H., Ahmad, Z., Kilany, M., Al-Shehri, B. M. and Al-Namshah, K. S. Novel Mg@ZnO nanoparticles synthesized by facile one-step combustion route for anti-microbial, cytotoxicity and photocatalysis applications. *J. Nanostruct. Chem.* **11**, 1 (2021).

[27] Hsiao, K.-Y., Chung, R.-J., Chang, P.-P. and Tsai, T.-H. Identification of Hydroxyl and Polysiloxane Compounds via Infrared Absorption Spectroscopy with Targeted Noise Analysis. *Polymers* **17**, 1533 (2025).

[28] Behrouzi, M. and Moghadam, P. N. Synthesis of a new superabsorbent copolymer based on acrylic acid grafted onto carboxymethyl tragacanth. *Carbohydr. Polym.* **202**, 227–235 (2018).

[29] Thombare, N., Mahto, A., Singh, D., Chowdhury, A. R. and Ansari, M. F. Comparative FTIR characterization of various natural gums: a criterion for their identification. *J. Polym. Environ.* **31**, 3372–3380 (2023).

[30] Babu, K. S., Reddy, A. R., Sujatha, C., Reddy, K. V. and Mallika, A. N. Synthesis and optical characterization of porous ZnO. *J. Adv. Ceram.* **2**, 260–265 (2013).

[31] Kanchana, S. K., Vanitha, N. and Basavaraj, R. B. Structural and optical properties of polyvinyl alcohol/copper oxide (PVA/CuO) nanocomposites. *Solid State Commun.* **370**, 115221 (2023).

[32] Nejatian, M., Abbasi, S. and Azarikia, F. Gum Tragacanth: Structure, characteristics and applications in foods. *Int. J. Biol. Macromol.* **160**, 846–860 (2020).

[33] Jangizehi, A., Schmid, F., Besenius, P., Kremer, K. and Seiffert, S. Defects and defect engineering in Soft Matter. *Soft Matter* **16**, 10809–10859 (2020).

[34] Folorunso, O., Hamam, Y., Sadiku, R. and Kupolati, W. Effects of defects on the properties of polymer nanocomposites: A brief review. *J. Inorg. Organomet. Polym. Mater.* **34**, 5667–5690 (2024).

[35] Vyas, A., Ng, S., Fu, T. and Anum, I. ZnO-Embedded Carboxymethyl Cellulose Bioplastic Film Synthesized from Sugarcane Bagasse for Packaging Applications. *Polymers* **17**, 579 (2025).

[36] Długosz, O. and Banach, M. Continuous synthesis of photocatalytic nanoparticles of pure ZnO and ZnO modified with metal nanoparticles. *J. Nanostruct. Chem.* **11**, 601–617 (2021).

[37] Zhao, Y., et al. Comprehensive review of polysaccharide-based materials in edible packaging: A sustainable approach. *Foods* **10**, 1845 (2021).

[38] Chen, J., Luo, L., Cen, C., Liu, Y., Li, H. and Wang, Y. The nano antibacterial composite film carboxymethyl chitosan/gelatin/nano ZnO improves the mechanical strength of food packaging. *Int. J. Biol. Macromol.* **220**, 462–471 (2022).

[39] Rezaei, F. T. M., Aryaee, P. and Abdullahi, M. Evaluation of some physical and mechanical properties of carboxymethyl cellulose/Tragacanth edible film. in *4th National Conference on Food Science and Technology* (Tehran, Iran, 2016).

[40] Rahman, M. S., et al. Recent developments of carboxymethyl cellulose. *Polymers* **13**, 1345 (2021).

[41] Fouad, H., Jawaid, M., Karim, Z. et al. Preparation and characterization of carboxymethyl microcrystalline cellulose from pineapple leaf fibre. *Sci Rep* **14**, 23286 (2024).

[42] Ahmed, M., Saini, P. and Iqbal, U. Microbial cellulose based films and composites for food packaging: A review. *Ann. Univ. Dunarea Jos Galati. Fascicle VI-Food Technol.* **45**, 178–198 (2021).

[43] Rezaei, F. T. M., Aryaee, P. and Abdullahi, M. Evaluation of some physical and mechanical properties of carboxymethyl cellulose/Tragacanth edible film. in *4th National Conference on Food Science and Technology* (Tehran, Iran, 2016).

[44] Bachra, Y., Grouli, A., Damiri, F., Talbi, M. and Berrada, M. A novel superabsorbent polymer from crosslinked carboxymethyl tragacanth gum with glutaraldehyde: synthesis, characterization, and swelling properties. *Int. J. Biomater.* **2021**, 5008833 (2021).

[45] Ahmed, M., Saini, P., Iqbal, U. and Sahu, K. Edible microbial cellulose-based antimicrobial coatings and films containing clove extract. *Food Prod. Process. Nutr.* **6**, 65 (2024).

[46] Gürler, N. and Ertekin, Ö. Physical and biological characteristics of eco-friendly films added with Cinnamomum zeylanicum extract for packaging materials. *Int. J. Food Sci. Technol.* **59**,

2400–2410 (2024).

[47] Rabeel, M., et al. Controlling the wettability of ZnO thin films by spray pyrolysis for photocatalytic applications. *Materials* **15**, 3364 (2022).

[48] Hammani, S., Daikhi, S., Bechelany, M. and Barhoum, A. Role of ZnO nanoparticles loading in modifying the morphological, optical, and thermal properties of immiscible polymer (PMMA/PEG) blends. *Materials* **15**, 8453 (2022).

[49] Mesgari, M., Aalami, A. H., Sathyapalan, T. and Sahebkar, A. A comprehensive review of the development of carbohydrate macromolecules and copper oxide nanocomposite films in food nanopackaging. *Bioinorg. Chem. Appl.* **2022**, 7557825 (2022).

[50] Rizal, S., et al. Cinnamon-nanoparticle-loaded macroalgal nanocomposite film for antibacterial food packaging applications. *Nanomaterials* **13**, 560 (2023).

[51] Zhao, J., Wang, Y. and Liu, C. Film transparency and opacity measurements. *Food Anal. Methods* **15**, 2840–2846 (2022).

[52] Chakka, V. P. and Zhou, T. Carboxymethylation of polysaccharides: Synthesis and bioactivities. *Int. J. Biol. Macromol.* **165**, 2425–2431 (2020).

[53] Jiang, L., et al. Effects of carboxymethyl modification on physicochemical properties, structure of fenugreek polysaccharide and its capabilities of aroma enhancement and moisture retention in cigarettes. *Int. J. Biol. Macromol.* **2025**, 146298 (2025).

[54] Badry, R., El-Nahass, M. M., Nada, N., Elhaes, H. and Ibrahim, M. A. Structural and UV-blocking properties of carboxymethyl cellulose sodium/CuO nanocomposite films. *Sci. Rep.* **13**, 1123 (2023).

[55] Mohammadifar, M. A., Musavi, S. M., Kiumarsi, A. and Williams, P. A. Solution properties of targacanthin (water-soluble part of gum tragacanth exudate from Astragalus gossypinus). *Int. J. Biol. Macromol.* **38**, 31–39 (2006).

[56] Mohammed, S. J., Al-Musawi, A. T., Al-Fraji, A. S. and Kareem, H. S. Comparison of three culture media in assessing the sensitivity of antibiotics to common foodborne microorganisms. *J. Med. Life* **15**, 645 (2022).

[57] Emamifar, A., Kadivar, M., Shahedi, M. and Soleimanian-Zad, S. Evaluation of nanocomposite packaging containing Ag and ZnO on shelf life of fresh orange juice. *Innov. Food Sci. Emerg. Technol.* **11**, 742–748 (2010).

[58] Sirelkhatim, A., et al. Review on zinc oxide nanoparticles: antibacterial activity and toxicity mechanism. *Nano-Micro Lett.* **7**, 219–242 (2015).

[59] Brand-Williams, W., Cuvelier, M. E. and Berset, C. Use of a free radical method to evaluate antioxidant activity. *LWT-Food Sci. Technol.* **28**, 25–30 (1995)

[60] Kedare, S. B. and Singh, R. P. Genesis and development of DPPH method of antioxidant assay. *J. Food Sci. Technol.* **48**, 412–422 (2011).

[61] Barton, H. J. A 'zero sample concentration approach': Standardization of methods for the estimation of total antioxidant activity by the use of extrapolation to zero sample concentration. A novel standard. 1. ABTS cation radical scavenging. *J. Agric. Food Chem.* **58**, 8918–8926 (2010).

[62] Munteanu, I. G. and Apetrei, C. Analytical methods used in determining antioxidant activity: A review. *Int. J. Mol. Sci.* **22**, 3380 (2021).

[63] Thangapandi, J. R., Chelliah, P., Balakrishnan, S., et al. Antibacterial and photocatalytic aspects of zinc oxide nanorods synthesized using Piper nigrum seed extract. *J. Nanostruct. Chem.* **11**, 549–560 (2021).

[64] Antosik, A. K., Bartkowiak, M., Zdanowicz, M. and Wilpiszewska, K. Carboxymethyl Polysaccharides/Montmorillonite Biocomposite Films and Their Sorption Properties. *Polymers* **17**, 2130 (2025).

[65] Zheng, S., et al. Implication of surface properties, bacterial motility, and hydrodynamic conditions on bacterial surface sensing and their initial adhesion. *Front. Bioeng. Biotechnol.* **9**, 643722 (2021).

[66] Zhang, H. and Nishinari, K. Characterization of the conformation and comparison of shear and extensional properties of curdlan in DMSO. *Food Hydrocoll.* **23**, 1570–1578 (2009).

[67] Hanani, Z. A. N., Roos, Y. H. and Kerry, J. P. Use of beef, pork and fish gelatin sources in the manufacture of films and assessment of their composition and mechanical properties. *Food Hydrocoll.* **29**, 144–151 (2012).

[68] Espitia, P. J. P., Soares, N. de F. F., Coimbra, J. S. dos R., de Andrade, N. J., Cruz, R. S. and Medeiros, E. A. A. Zinc oxide nanoparticles: synthesis, antimicrobial activity and food packaging applications. *Food Bioprocess Technol.* **5**, 1447–1464 (2012).

[69] Grabowski, N. T. and Klein, G. Bacteria encountered in raw insect, spider, scorpion, and centipede taxa including edible species, and their significance from the food hygiene point of view. *Trends Food Sci. Technol.* **63**, 80–90 (2017).

[70] Duncan, T. V. Applications of nanotechnology in food packaging and food safety: barrier materials, antimicrobials and sensors. *J. Colloid Interface Sci.* **363**, 1–24 (2011).

[71] Cushen, M., Kerry, J., Morris, M., Cruz-Romero, M. and Cummins, E. Evaluation and simulation of silver and copper nanoparticle migration from polyethylene nanocomposites to food and an associated exposure assessment. *J. Agric. Food Chem.* **62**, 1403–1411 (2014).

[72] Rhim, J.-W. and Ng, P. K. W. Natural biopolymer-based nanocomposite films for packaging applications. *Crit. Rev. Food Sci. Nutr.* **47**, 411–433 (2007).

[73] Anal, A. K. and Singh, H. Recent advances in microencapsulation of probiotics for industrial applications and targeted delivery. *Trends Food Sci. Technol.* **18**, 240–251 (2007).

[74] Bachra, Y., Grouli, A., Damiri, F., Talbi, M. and Berrada, M. A novel superabsorbent polymer from crosslinked carboxymethyl tragacanth gum with glutaraldehyde: synthesis, characterization, and swelling properties. *Int. J. Biomater.* **2021**, 5008833 (2021).